SKB

Checking the consistency of the "two-zone model" for Task 9B – LTDE-SD

Task 9 of SKB Task Force GWFTS – Increasing the realism in solute transport modelling based on the field experiments REPRO and LTDE-SD

Klaus-Peter Kröhn

SVENSK KÄRNBRÄNSLEHANTERING

Checking the consistency of the "two-zone model" for Task 9B – LTDE-SD

Task 9 of SKB Task Force GWFTS – Increasing the realism in solute transport modelling based on the field experiments REPRO and LTDE-SD

Klaus-Peter Kröhn

Gesellschaft für Anlagen- und Reaktorsicherheit (GRS) gGmbH

Abstract

The Long-Term Diffusion Experiment (LTDE) was commenced in 2006 at the Äspö Hard Rock Laboratory in Sweden. By a complex set of drilling stages and instrumentations, a solution containing different ionic solutes was circulated allowing for diffusion of the tracers into the crystalline rock from a borehole as well as from a natural fracture.

When the experiment was terminated in 2007, the tracer concentration profiles reaching into the rock were determined in the laboratory. The resulting profiles had not the anticipated smooth shape, though, but appeared to be rather crooked and reaching almost plateau-like deeply into the rock. In the framework of SKB's Task Force on Groundwater Flow and Transport of Solutes, many fundamentally different approaches have been brought forward to explain the findings.

The work described in this report focusses on a model that is potentially viable from an engineering point of view, checking stringently the consistency of the available data and the model results. It is based on the concept of a narrow zone at the contact of rock and solution that is different from the undisturbed matrix beyond. As the model is the more meaningful, the less parameters are used for fitting the measurements, the number of fitting parameters was kept to a minimum.

A detailed and in-depth analysis of the data suggested that only the profiles for $^{22}Na^+$, $^{36}Cl^-$, $^{137}Cs^+$, $^{133}Ba^{2+}$, and $^{57}Co^{2+}$ were relevant for this investigation. Work on $^{57}Co^{2+}$ had to be dropped due to time limitations, though. Furthermore, the data from the different drill cores suggest a surprisingly high degree of inhomogeneity of the rock on the scale of less than a decimeter.

The fitting procedure was subject to several restrictions that followed from the approach of the two-zone model. In case of the cation tracers, the one value for porosity and tortuosity, respectively, of the undisturbed matrix used in all models came indeed reasonably close to expectations. For $^{36}Cl^-$, however, these values were much lower, suggesting anion exclusion by very narrow pore channels in the rock.

By and large, the parameters derived from the fitting procedure explain the tracer profiles reasonably well, thereby confirming the plausibility of the proposed two-zone approach. However, this result must not be mistaken for a proof of concept as there are many other potentially viable explanations for the curious tracer profiles.

Sammanfattning

Long-Diffusion Experiment (LTDE) inleddes 2006 på Äspö Hard Rock Laboratory i Sverige. Genom en komplex uppsättning borrningar och instrumentering cirkulerades en lösning innehållande olika joniska lösta ämnen som möjliggjorde diffusion av spårämnen till det kristallina berget från ett borrhål samt från en naturlig spricka.

När experimentet avslutades 2007 bestämdes koncentrationsprofiler av de spårämnen som når in i berget via laboratoriemätningar. De resulterande profilerna hade dock inte den förväntade formen, men tycktes vara nå nästan platåliknande kurvor djupt in i berget. Inom ramen för SKB: s Task Force för grundvattenflöde och transport av lösta ämnen har många grundläggande och olika tillvägagångssätt tagits fram för att förklara resultaten.

Arbetet som beskrivs i denna rapport fokuserar på en modell som är potentiellt hållbar ur en teknisk synvinkel och strängt kontrollerar överensstämmelsen mellan tillgängliga data och modellresultaten. Den är baserad på ett koncept baserat på en smal zon vid kontaktytan mellan berg och vattenlösningen som skiljer sig från den ostörda bergsmatrisen längre bort. Eftersom modellen är desto mer meningsfull, desto färre parametrar som används för anpassning till mätningarna, hölls antalet passningsparametrar till ett minimum.

En detaljerad och djupgående analys av experimentella data antydde att endast profilerna för ^{22}Na$^+$, ^{36}Cl$^-$, ^{137}Cs$^+$, ^{133}Ba^{2+} och ^{57}Co^{2+} var relevanta för denna undersökning. Arbetet med ^{57}Co^{2+} utfördes dock inte på grund av tidsbegränsningar. Vidare antyder data från de olika borrkärnorna en överraskande hög grad av inhomogenitet hos berget i skalan mindre än en decimeter.

Passningsförfarandet var föremål för flera begränsningar som var en följd av tillvägagångssättet för tvåzonsmodellen. För katjoner var värdena för porositet respektive tortuositet för den ostörda matrisen, som användes i alla modeller, rimligt nära de förväntade. För ^{36}Cl$^-$ var emellertid dessa värden mycket lägre, vilket tyder på att anjoner utesluts i de mycket smala porkanalerna i berget.

I stort förklarar parametrarna som härrör från passningsproceduren spårämnesprofilerna rimligt väl och bekräftar därmed rimligheten för den föreslagna metoden med två zoner. Detta resultat får emellertid inte misstas som ett bevis på att konceptet gäller eftersom det finns många andra möjliga förklaringar för de märkliga spårämnesprofilerna.

Contents

1 Background

1.1 The LTDE experiment

The Long-Term Diffusion Experiment (LTDE) – a sketch is shown in Figure 1-1 – had been carried out at the Hard Rock Laboratory (HRL) Äspö in Sweden. Objective of the experiment was to check the concepts of diffusion and sorption of radioactive nuclides in crystalline rock. By a complex set of drilling stages and instrumentation (see Figure 1-2 and Figure 1-3), a solution containing 22 different solutes[1] was circulated across a circular part of a fracture surface as well as in a cylindrical borehole beyond the fracture. The cylindrically encased piece of rock at the fracture is called "stub".
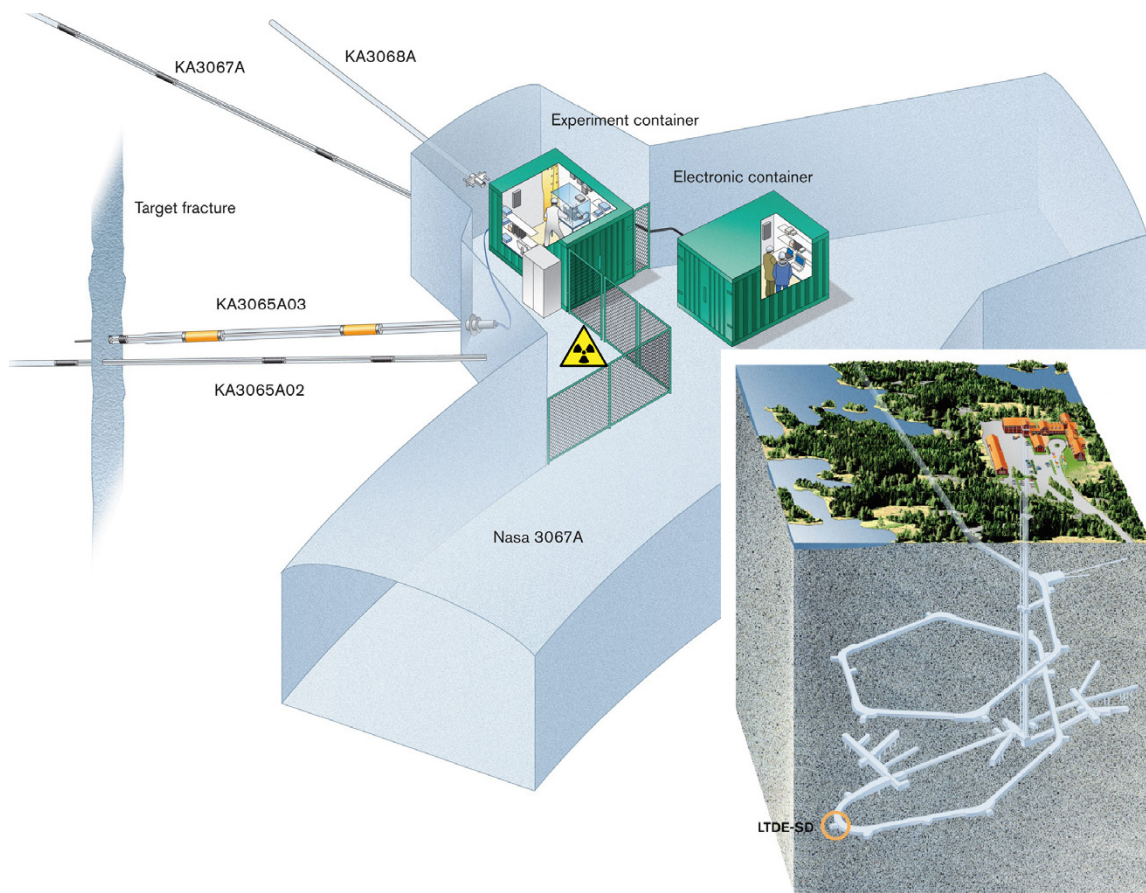
Figure 1-1. *Location of the LTDE-Experiment; from Widestrand et al. (2010a).*

---

[1] ^{22}**Na**$^+$, ^{35}SO$_4$$^{2-}$, ^{36}**Cl**$^-$, ^{57}**Co**$^{2+}$, ^{63}**Ni**$^{2+}$, ^{75}SeO$_4$$^{2-}$, ^{85}Sr^{2+}, ^{95}NbO^{2+}, ^{95}Zr^{4+}, ^{99}TcO$_4$$_-$, ^{102}Pd^{2+}, ^{109}**Cd**$^{2+}$, ^{110m}**Ag**$^+$, ^{113}Sn^{4+}, ^{133}**Ba**$^{2+}$, ^{137}**Cs**$^+$, ^{153}**Gd**$^{3+}$, ^{175}Hf^{4+}, ^{226}**Ra**$^{2+}$, ^{233}PaO(OH)$_3$, ^{236}UO$_2$$^-$, and ^{237}**NpO**$_2$$_+$. The tracer names written in bold were considered in Task 9b. Data relevant for modelling can be found in Appendix 1.

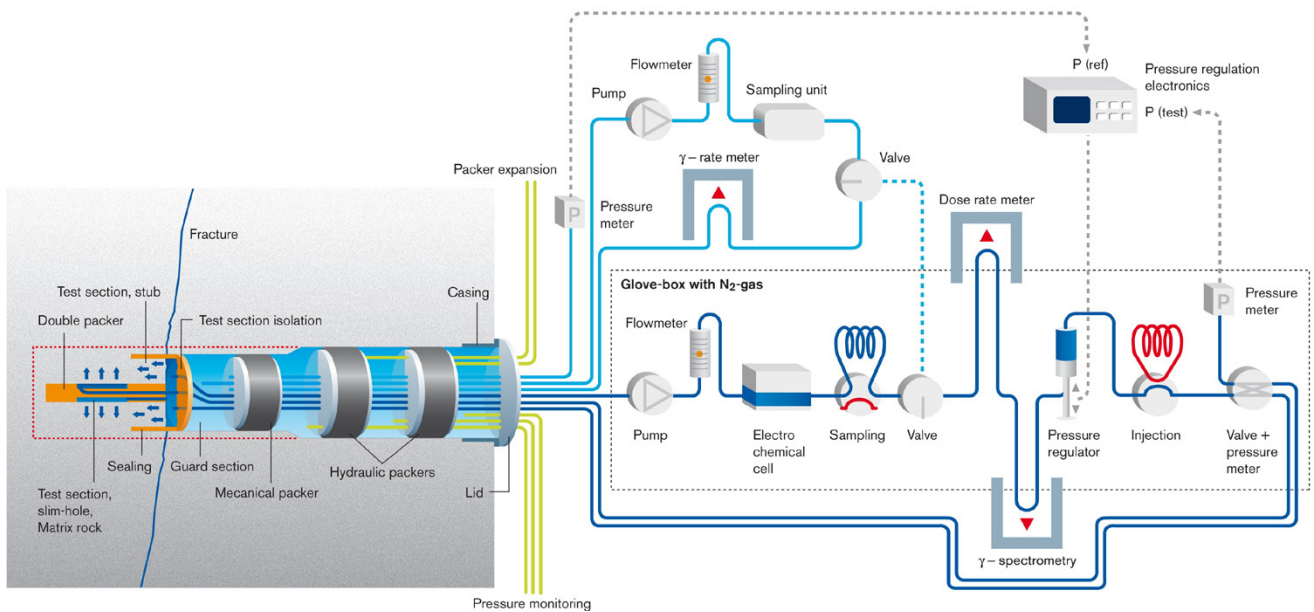***Figure 1-2.*** *Borehole instrumentation and test section design; from Widestrand et al. (2010b).*
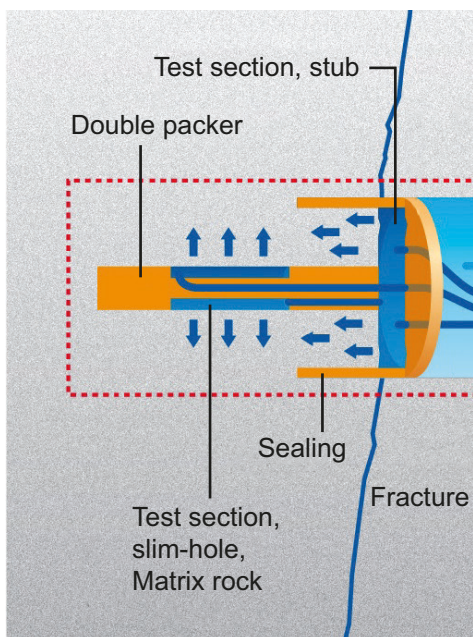

Figure 1-3. *Test sections, close-up from Figure 1-2; modified from Widestrand et al. (2010b).*

The tracer concentration in the test sections was monitored during the experiment. As the tracers were not replenished a decline in the concentration over time was expected. As it turned out, the concentration of the tracers $^{57}Co^{2+}$, $^{110m}Ag^+$, and $^{153}Gd^{3+}$ decreased by several orders of magnitude while the concentration of the other tracers can reasonably well be approximated by a constant even if not necessarily the initial value. For details see Appendix 2.

When the experiment was terminated the inflow reservoir was filled with resin in order avoid further diffusion of tracers into the rock. Borehole and stub were overcored. After a certain delay small cylindrical cores were drilled according to the pattern depicted in Figure 1-4 and sealed. Relevant for the task at hand were the A-cores that were drilled through the fracture surface and were therefore arranged in parallel as well as the D-cores taken in radial direction from the borehole axis.

Figure 1-4. *Drill pattern of the overcored inflow reservoir; from Nilsson et al. (2010).*

After another delay period the cores were sliced following a complex procedure which led to sub-samples as illustrated in Figure 1-5. The thickness of the slices varied and is listed in Table 1-1. The tracer concentrations were then determined in the subsamples by means of a number of analysis methods. These include autoradiography on intact samples, direct activity measurements on intact as well as crushed samples, and leaching or dissolution of intact and crushed samples, followed by water phase measurements.

The timeline of events that are relevant for modelling is given in Table 1-2 together with the duration of the periods and a related model time.

Figure 1-5. *Slicing pattern of the drill cores; from Nilsson et al. (2010).*

Table 1-1. Thickness of slices according to slicing plan.

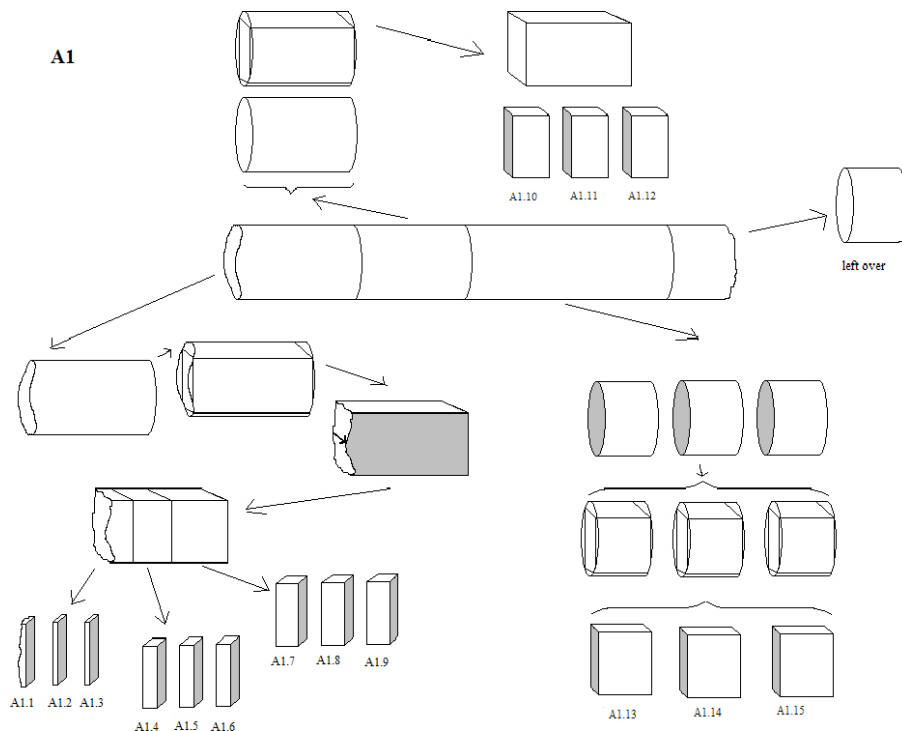| Slice #	1[2]	2	3	4	5	6	7	8	9	10	11	12
Thickness [mm]	> 1	1	1	3	3	3	5	5	5	10	10	10
Data allocation [mm]	(>) 0.5	1.5	2.5	4.5	7.5	10.5	14.5	19.5	24.5	32	42	52

Table 1-2. Timeline of the experiment, period lengths and resulting model times.

Date	Action	Duration [d]	Model time [d]
27.09.2006			
27.09.2006	begin of LTDE		0
	LTDE	197	
12.04.2007	end of LTDE		197
	delay until drilling	120	
10.08.2007	middle of drilling		317
	delay until slicing	76	
25.10.2007	begin of slicing		393
	slicing	128	
01.03.2008	end of slicing		521

The resulting concentration profiles had not the anticipated shape. Up to three different characteristic parts of the curve were found. Mostly, the concentration decreased from the rock surface with a steep gradient over the first few millimetres into the rock. Subsequently, the gradient changed quite suddenly to a much lower slope followed eventually by a more or less horizontal plateau. A typical result is shown in Figure 1-6 for $^{226}Ra^{2+}$. However, not all of the three parts could be observed in all activity curves.

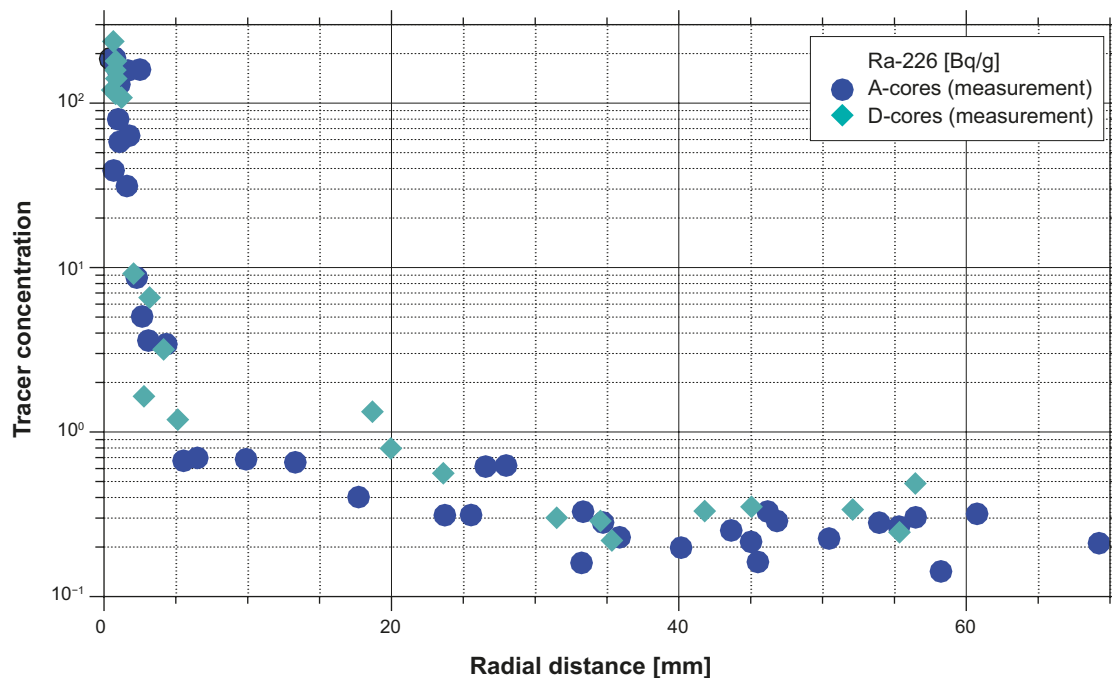**Figure 1-6.** $^{226}Ra^{2+}$ *tracer profile found to be characteristic for the LTDE[3].*

---

[2] Includes the rough core face surface.

[3] Note that throughout this report, the mass specific concentration refers to the mass of rock.

1.2   Motivation

The reason for setting up the LTDE as Task 9b in the framework of the Task Force on Groundwater Flow and Transport of Solutes (TF GWFTS) of the Svensk Kärnbränslehantering (SKB) was that no obvious and convincing mechanism had been found to explain the curious concentration curves (Löfgren and Nilsson 2020). The interest of GRS in joining Task 9b had been to check the own d³f++ code using real data of advanced hydrochemical processes. In the run-up to Task 9 it had for instance been speculated that interaction of tracers might have played a role thus calling for a smart K_d-approach which is actually realised in the d³f++ code. As it turned out, though, there was not enough data available to run the smart K_d-option. Apart from that there was a general bafflement about the physical explanation of the curious tracer profiles. The focus of GRS thus shifted towards finding a plausible mechanism.

1.3   Explanations for the data

Over time, many different approaches have been brought forward by the participants of the TF GWFTS. They are shortly described in the following to illustrate the great uncertainty that the LTDE-results had caused. The sequence in which the approaches are listed is not prioritising their credibility or their success. The suggesting party is labelled in brackets.

– Homogeneous matrix with kinetic sorption (KTH).

– Multi-zone models, optionally including the reservoir. Intuitively, one can assume that the tracers pass sequentially through two zones with different transport parameters. These zones could be interpreted as a skin zone and the undisturbed rock. The skin zone would have to show a much less apparent diffusivity than the neighbouring zone (see Section 1.4) (TUL, KTH, JAEA, KAERI, LANL).

An interesting refinement has been brought forward by KAERI who combined the multi-zone model with a detailed description of the rock – including the disturbed zone – on the micro-scale (see also mineralogical heterogeneities on micro-scale) and above that with an additional microfracture.

By contrast, LANL postulated a disturbed zone represented by a micro-DFN (see below) in a continuous matrix, followed by a homogeneous matrix.

– Double continuum models. It has been speculated that there could be two parallel domains with different transport parameters that might be constituted by channels or fractures with different channel widths/fracture apertures as this would mathematically explain the concentration curves (HYRL, TUL).

– Mineralogical heterogeneities on micro-scale. These are grain scale models where the grains had been located and identified by X-ray tomography and each type of grain has a different sorption capacity. (CFE, AMPHOS, TUL, HYRL, KAERI (see also multi-scale models)).

– Micro-DFN (ProGeo, LANL (see also multi-scale models)).

– Advection towards the borehole (GRS).

– Degassing. Evolution of dissolved gases under decreasing hydraulic pressure (SU, GRS).

– Artefacts.

  • Capillary transport during drying of the overcored rock sample (KTH).

  • Contamination by drilling and sawing. May have happened if drilling or sawing was done from high to low tracer concentrations (GeoSigma).

  • Challenge of the dispersion concept. Applying Taylor-dispersion thus including effects on pore scale was suggested (KTH).

  • Electromigration. Movement of ions along an electrical potential gradient like the one produced by the High Voltage Direct Current (HVDC) transmission between Gotland and the main land just 16 km away from Äspö (Niressa).

Abbreviations for the contributing teams

AMPHOS   – AMPHOS[21], Barcelona

CFE   – Computer-aided Fluid Engineering (CFE) AB, Lyckeby

Geosigma   – Geosigma AB, Uppsala

GRS   – Gesellschaft für Anlagen- und Reaktorsicherheit gGmbH, Braunschweig

HYRL   – Helsingin Yliopista – Universität Helsinki

JAEA   – Japan Atomic Energy Agency, Tokyo

KAERI   – Korea Atomic Energy Research Institute, Daejeon

LANL   – Los Alamos National Laboratory, Los Alamos

Niressa   – Niressa AB, Norsborg

PROGEO   – ProGeo, s.r.o., Prag

TUL   – Technische Universität Liberec

1.4   Workshop on the skin-effect

In the framework of Task 8 GRS had used a narrow and flow-impeding zone around geotechnical openings in order to explain the comparatively low outflow from the rock (Kröhn 2018). This effect was included ad-hoc as it had already been observed during the Two-Phase Flow Project at the HRL Äspö (Kull et al. 2002). The observation could not be explained but was later commonly referred to as the "skin-effect".

Incorporating a skin in the GRS flow models for the BRIE and the Prototype Repository intrigued the participants of the TF GWFTS. Since a similar effect was suspected to influence the results from the LTDE in the parallel running Task 9b it was decided to organise a separate workshop on the skin-effect during the meeting in Prague in 2016 in order to benefit from the gathered knowledge among the TF participants. 13 contributions covered 20 examples from 7 underground laboratories (URL) in 5 countries worldwide, from laboratories and modelling exercises. The presentations were evaluated and the abstracts together with the results compiled in Kröhn and Lanyon (2018).

In the report the contents are divided according to the affected repository-relevant processes, namely groundwater flow and solute transport, because the spatial scale of the related observations is quite different. While a flow skin, as a general rule, appears to be associated with scales on the order of a metre, the observed transport skins have a thickness on the mm- to cm-scale.

From the compiled observations it is believed that no single cause explains all the observations and that in some cases it is possible that multiple processes and features of the flow system interact to cause observed skin effects. Unfortunately, the proposed explanations for skin can in many cases not be quantified for a specific situation. Often crucial information is missing, even in well-controlled environments. For these reasons typically only qualitative descriptions of the observed effects could be given and predictive models are (still) absent entirely. Spending a lot of effort, the workshop had thus brought forward valuable insight into the possibly "significantly under-reported" skin-effect(s) but not the much hoped-for conclusive explanation for the curious concentration profiles in the LTDE.

2   Approach

Left with no clear concept after some time of Task 9b had already elapsed and with the notion that sheer data fitting to an abstract model appeared to be pointless, it was no longer looked for a single convincing explanation of the tracer profiles. GRS therefore shifted the focus of the work towards a model that was potentially viable from an engineering point of view in order to check stringently the viability with the available data.

The skin-workshop had made clear that a transport skin might be caused by the drilling of the test borehole. The cooling fluid containing fine particles might have superficially clogged the pore space in the rock at the borehole wall. Also, a borehole disturbed zone (BDZ) might have developed causing a larger surface area for sorption. The fracture surface could clearly not have been affected by drilling but showed a coating from mineralisation. These considerations suggest a two-zone model with a narrow zone at the contact of rock and solution and an undisturbed matrix beyond as an appropriate representation of the situation at the LTDE. Further work is based on this assumption.

The strategy of choice was to fit the model results to the data and then to check if the resulting parameters make sense assuming that the data had not been compromised by contamination during the measurements. The result of this exercise is obviously the more meaningful the less parameters are used for the fitting, meaning that the number of fitting parameters for the model should be as small as possible. It helped therefore that the properties of the undisturbed matrix are comparatively well-known thus leaving little leeway for fitting in this part of the model.

The envisaged modelling procedure was kept straightforward and thereby hopefully robust. It took place in two steps. In the first step transport of a non-sorbing tracer was to be modelled in order to find out about the pore space topology. The only candidate was the anion $^{36}Cl^-$. All other tracers were cations that are prone to sorption because of the negative surface charge density of the crystalline rock. However, an effect from anion exclusion in narrow pore channels on the $^{36}Cl^-$–tracer could not be ruled out entirely.

Without sorption, the only transport-relevant mechanism is diffusion. Fick's second law could therefore be applied in case of $^{36}Cl^-$:

$$\Phi \frac{\partial c}{\partial t} - \Phi \, \tau^+ \, \nabla \cdot \left(D \nabla c \right) = 0 \tag{2-1}$$

Φ – porosity [-]

c – tracer concentration [-]

t – time [s]

τ^+ – factor comprising diffusion limiting influences (tortuosity, constrictivity etc) [-]

D – diffusion coefficient [m²/s]

Assuming a homogeneous domain, only the diffusion limiting factor τ^+ remains for fitting since the diffusion coefficient is well-known and the porosity cancels out. Note that all activity data are given as decay-corrected. Meaning and purpose are that the measured data was transformed to values as if no decay had taken place to allow for including codes that do not consider radioactive decay.

Adding a disturbed zone to the model increases the number of fitting parameters because the factor τ^+ cannot be expected to be the same in both parts of the model. The same applies to the porosity meaning that the porosity does not cancel out of the diffusion equation anymore. Two more parameters concern the disturbed zone. First, there is the unknown depth of the disturbed zone. Thinking of clogging from drilling fluid fines and/or mechanical disturbances from drilling, it appears to be highly improbable that the pore space geometry in disturbed zone is constant all over this zone and just simply switching at the zone boundary. Rather a transition of the parameters from the sample surface to the not affected matrix is expected. This transition can be formulated as a factor that depends on the distance from the surface and the depth of the disturbed zone:

$$\Phi_{matrix} + \left(\frac{l-x}{l}\right)^m \cdot \Delta\Phi = 0 \qquad (2\text{-}2)$$

l — depth of the disturbed zone [m]

m — exponent [-]

$\Delta\Phi$ — maximum difference of the porosity between BDZ and matrix [-]

x — distance to the sample surface [m]

The same can analogously be formulated for the parameter τ^+. Different shapes of the transition function can be achieved by varying the exponent m. Examples for a normalised depth are given in Figure 2-1.
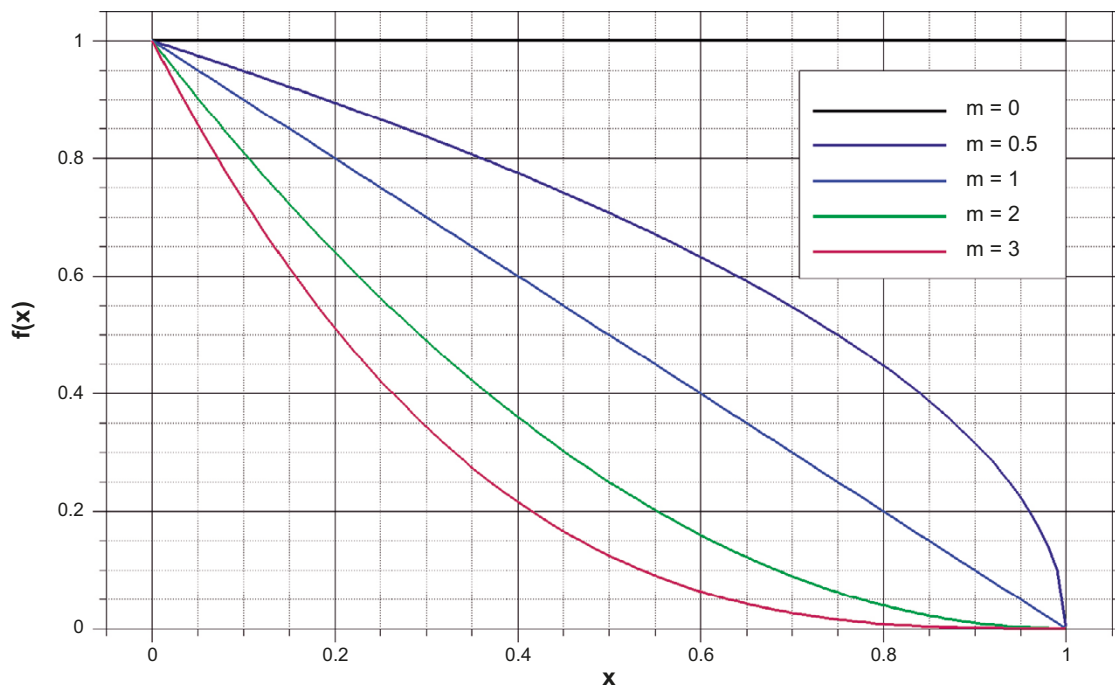

Figure 2-1. *Examples for the transition function for a normalised depth.*

Calibrating the model for ^{36}Cl$^-$-migration with respect to these six parameters takes care of the geometrical aspect of the porous transport system. Modelling migration of the cations should therefore add only sorption to the problem:

$$\left(\Phi+\left[1-\Phi\right]\rho_s K_d\right)\frac{\partial c}{\partial t}-\Phi\,\tau^+\nabla\cdot\left(D\nabla c\right)=0 \tag{2-3}$$

K_d — distribution coefficient for equilibrium sorption [m³/kg]

Step 2 is thus concerned with the cations thereby including sorption. As the K_d-value for all tracers has been determined in the laboratory this should not add a new fitting parameter. In an ideal case, the models for anion transport should immediately work with the known parameters from the calibrated model for ^{36}Cl$^-$. Note that the topological parameters for the matrix should be the same for the models of the A-cores and the D-cores.

2.1   Data analysis

Activity data for the eleven tracers chosen for investigation in Task 9b had been provided. A detailed and in-depth analysis of the data is given in Appendix 4. The main observations and conclusions from that analysis are:

(1): The detection limits are related to the subsample sizes as indicated in Figure 2-2. If the activity values are in the same range and show the same trend as the detection limits as in case of ^{226}Ra^{2+} the activity data become meaningless. Concentration values that lie at the detection limits must therefore be considered to be at least comparatively badly known.

As the scatter in the data at the detection limits might indicate an indeterminable continuation of the concentration distribution below the detection limits it is no use to discuss model results in the range of such data. This applies even more so to domain sections where all concentration values lie below the detection limits because they are entirely unknown and could even be zero if no tracer material has reached the particular position at all.
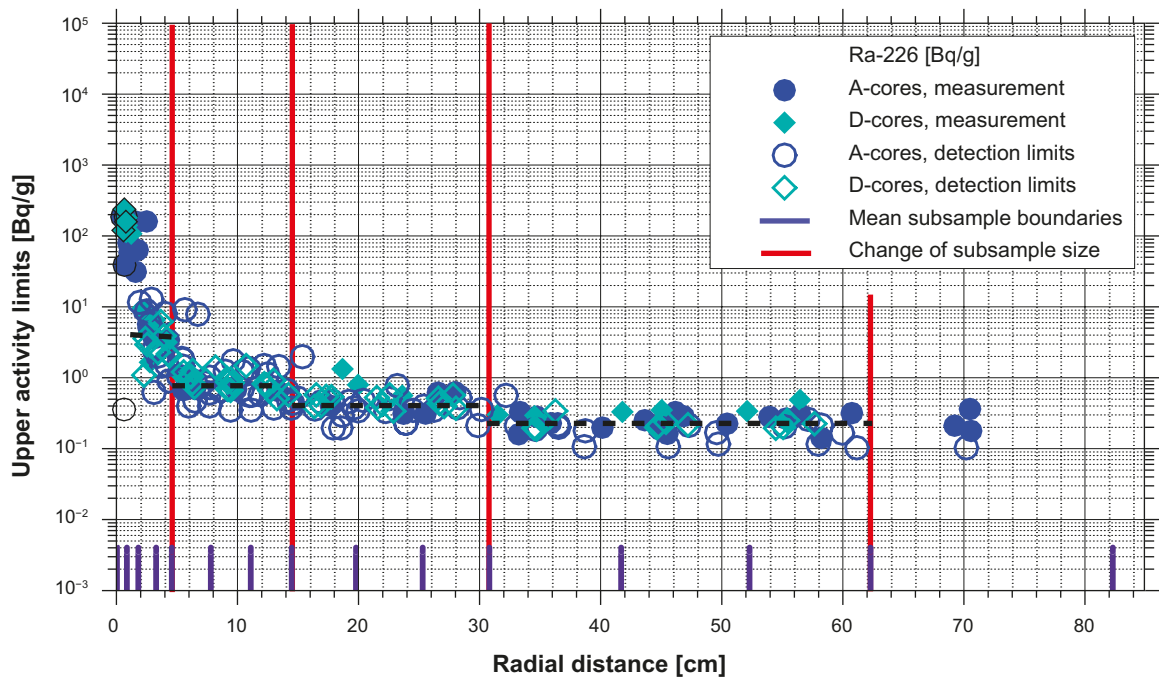

Figure 2-2. *^{226}Ra^{2+} tracer profile, detection limits and subsample partitioning.*

(2): Only the activity data for $^{22}Na^+$, $^{36}Cl^-$, and $^{137}Cs^+$ are entirely and for $^{57}Co^{2+}$ and $^{133}Ba^{2+}$ at least partially relevant in that the data points lie clearly above the detection limits. All others show significant values only within a few millimeters from the borehole wall/fracture surface and are therefore not used for modelling.

(3): Data for $^{36}Cl^-$ and $^{22}Na^+$ from the D-cores do not show the steep concentration gradient in the immediate vicinity of the former reservoir. This observation is most significant as it indicates a principal difference between the fracture surface and the borehole wall and thus calls for different models for A- and D-cores.

(4): There is much less data uncertainty within a drill core than scatter between the cores. Apparently, there is already considerable local variation of material properties in the matrix on the scale of the LTDE. Fitting model results to the data can therefore not be done as stringent as it had been hoped for.

Based on these observations, only the tracers $^{22}Na^+$, $^{36}Cl^-$, $^{137}Cs^+$, and $^{133}Ba^{2+}$ were investigated. Work on $^{57}Co^{2+}$ had to be dropped due to time limitations.

2.2 Homogeneous model

The attempt to fit model results and tracer data with a homogeneous model failed as in earlier modelling exercises (e.g. Nilsson et al. 2010). The only available fitting factor τ^+ (see Section 2) just changes the curvature of the calculated curves and particularly not the starting point at the sample surface, so the result shown in Figure 2-3 is close to the best fit. The three tracers depicted in Figure 2-3 represent two slightly different trends for $^{36}Cl^-$ in the D-cores as discussed at the end of Appendix 4 in more detail. Both are not even close to the numerical result. Note that the tracer concentrations depicted in Figure 2-3 to Figure 3-9 as well as Figure A4-1 to Figure A4-10 in Appendix 4 are given in Bq per gram of rock.
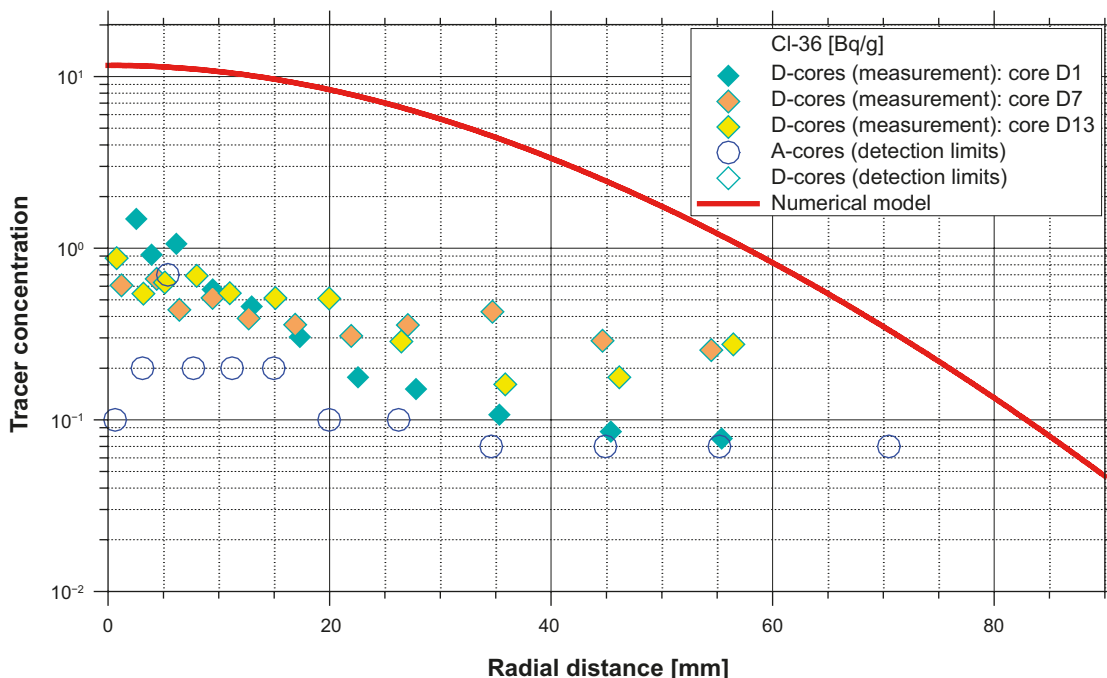

Figure 2-3. *Best model fit of a homogeneous model to the $^{36}Cl^-$-data from the D-cores.*

3 Results for the two-zone model

3.1 Fitting results for A-cores

Since structural differences between the A-cores and the D-cores were suspected (see Section 2) fitting was done for the A-cores and later separately for the D-cores. Step 1 – fitting the results for $^{36}Cl^-$ – resulted in the fit shown in Figure 3-1.

As it turned out, though, this particular data set was the only one suggesting a disturbed zone as large as 5 mm. Moreover, the matrix porosity and tortuosity were extremely low (0.0004 and 0.005, respectively) which seems to indicate that there is actually some anion exclusion having effect in the matrix. What this means for the disturbed zone is not clear. For the fitting strategy, however, it means that the data for $^{36}Cl^-$ cannot be used as a basis for fitting the profiles for the cations.
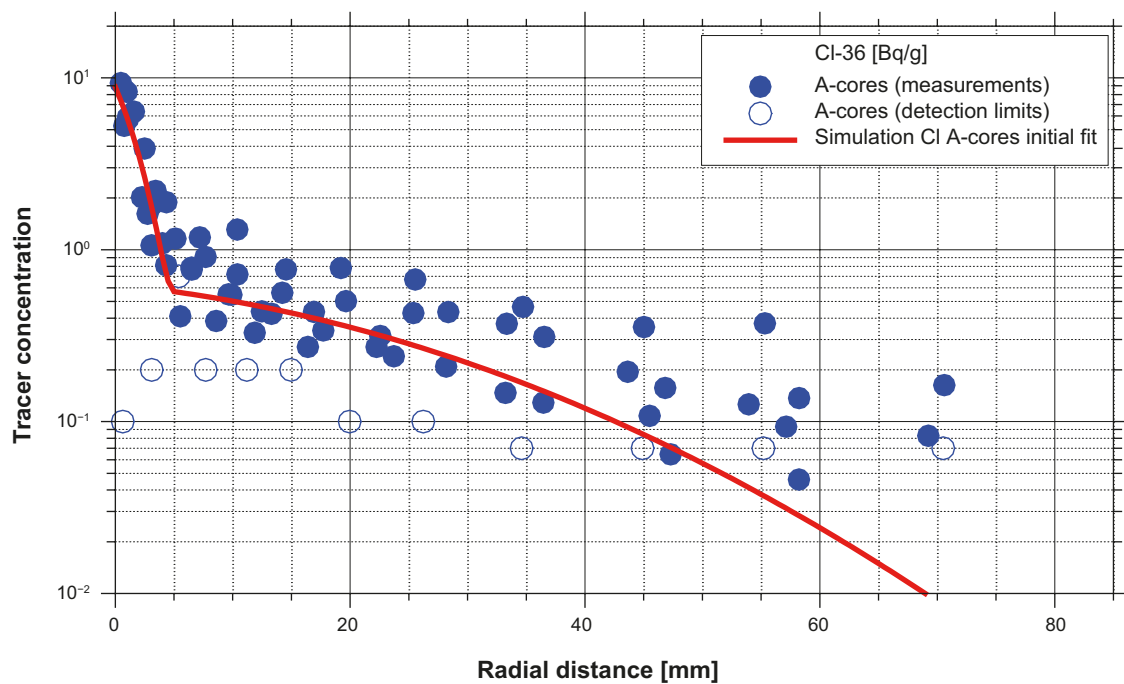

Figure 3-1. *Fit of the two-zone model to the $^{36}Cl^-$ data set from the A-cores; initial fit.*

Since the goal was to use one and the same parameter set for all data, the models for the three cations in the A-cores were fitted next and then reconciled with the $^{36}Cl^-$–profile. Fitting the results for the three cations (see Figure 3-3 to Figure 3-5) worked out well. In case of $^{137}Cs^+$ (see Figure 3-4) re-evaluation of the data determination by Geosigma led to an increase of the detection limits as indicated by a dashed blue line which made the fitting a much better one. The topological parameters from the fitting exercise remained to be quite different for $^{36}Cl^-$ and the three cations as the compilation in Table 3-1 shows, confirming the suspicion of anion exclusion. The good fit for $^{36}Cl^-$ as in Figure 3-1 could not be achieved after applying a data set common for all tracers even allowing for differences in the matrix as shown in Figure 3-2.

Nevertheless, the data in Table 3-1 show reasonable values for matrix porosity and tortuosity (0.004 and 0.4, respectively). In comparison, the data for the disturbed zone a slightly decreased porosity (0.003) and a strongly decreased tortuosity (0.0006) which underpins the notion of a pore space filled with fines.

Table 3-1. Fitting parameters for the model results depicted in Figure 3-2 to Figure 3-5[4].

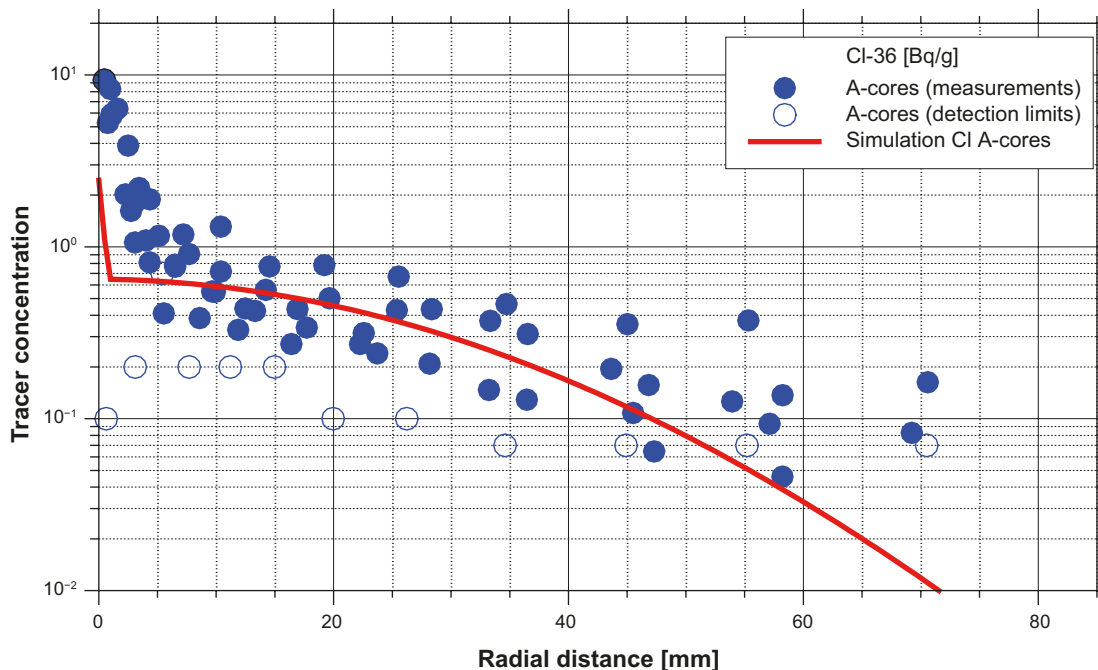| A-cores	$^{36}Cl^-$	$^{22}Na^+$	$^{137}Cs^+$	$^{133}Ba^{2+}$
Φ_{BDZ} [-]	0.003	0.003	0.003	0.003
τ^+_{BDZ} [-]	0.0006	0.0006	0.0006	0.0006
l_{BDZ} [mm]	1	1	1	1
Φ_{matrix} [-]	0.0008	0.004	0.004	0.004
τ^+_{matrix} [-]	0.005	0.4	0.4	0.4
m [-]	2	2	2	2

Figure 3-2. *Fit of the two-zone model to the $^{36}Cl^-$ -data set from the A-cores.*

---

[4] The index "BDZ" denotes the narrow zone at the rock surface while the index "matrix" stands for the undisturbed matrix.
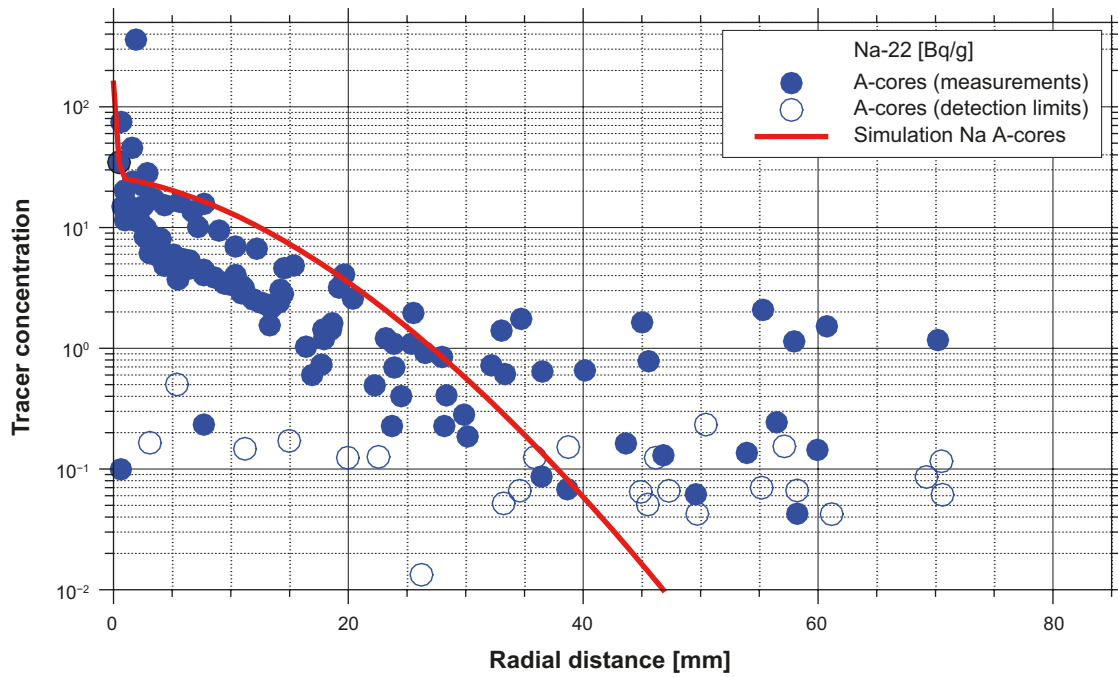
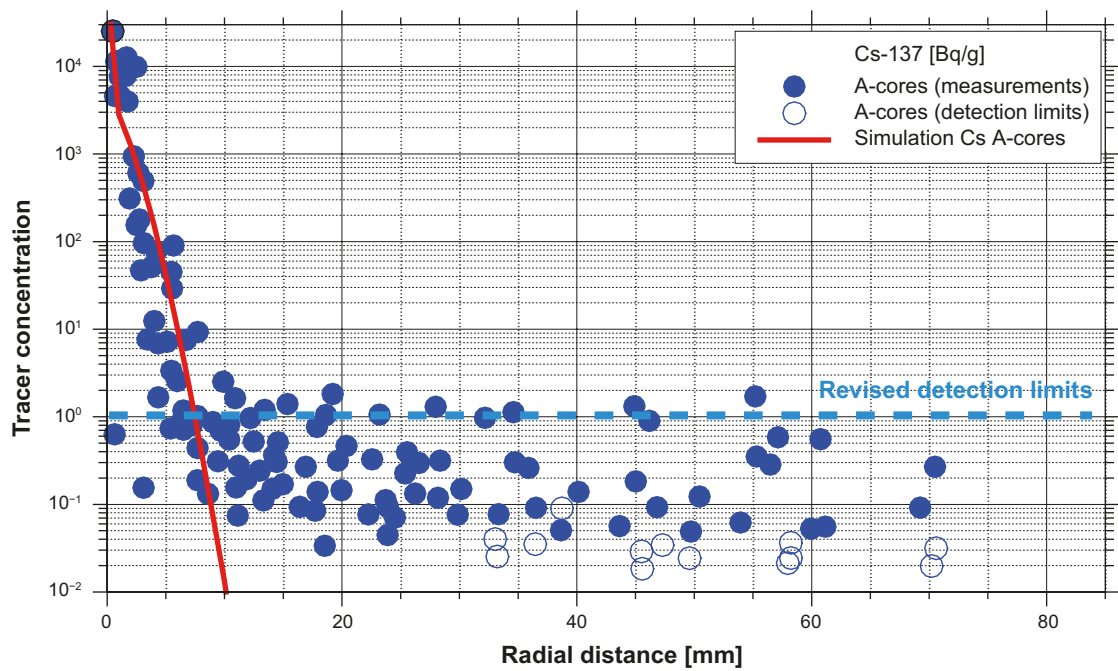**Figure 3-3.** *Fit of the two-zone model to the $^{22}Na^+$-data set from the A-cores.*

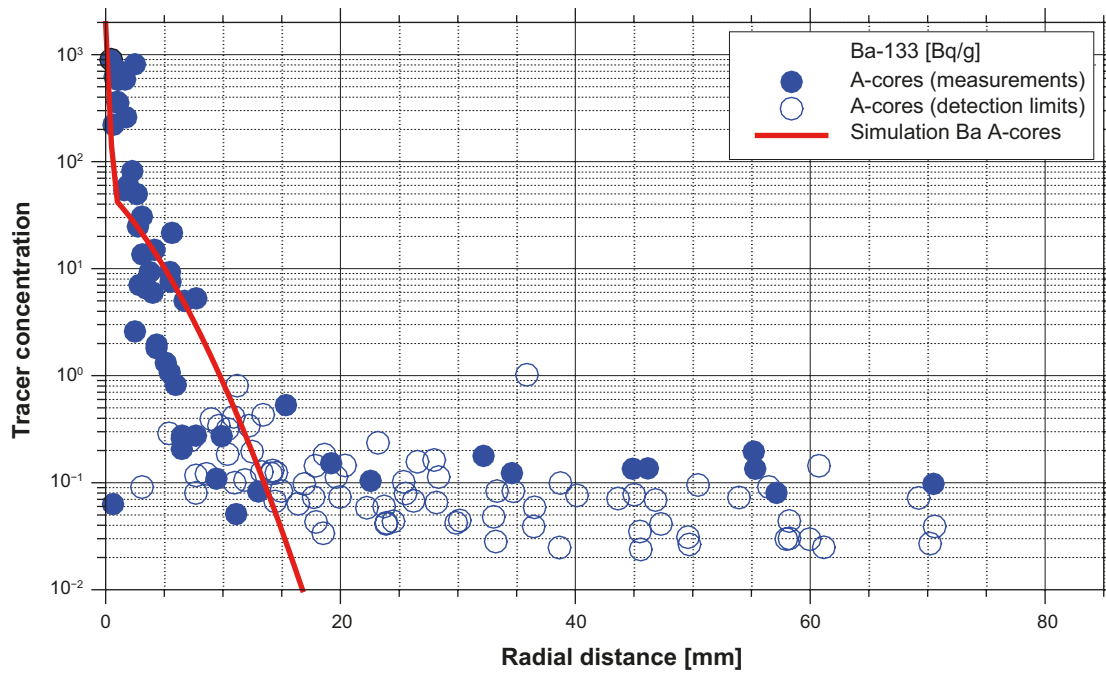**Figure 3-4.** *Fit of the two-zone model to the $^{137}Cs^+$-data set from the A-cores.*

Figure 3-5. *Fit of the two-zone model to the $^{133}Ba^{2+}$-data set from the A-cores.*

3.2 Fitting results for D-cores

The procedure described in the previous section was repeated for the D-cores. However, the results and conclusions are in principle the same as illustrated by Table 3-2 and Figure 3-6 to Figure 3-9. Note that the approach is more or less able also to account for the tracer profiles that do not show the initial steep concentration gradient as for $^{36}Cl^-$ and $^{22}Na^+$ (see Figure 3-6 and Figure 3-7).

Table 3-2. Fitting parameters for the model results depicted in Figure 3-6 to Figure 3-9.

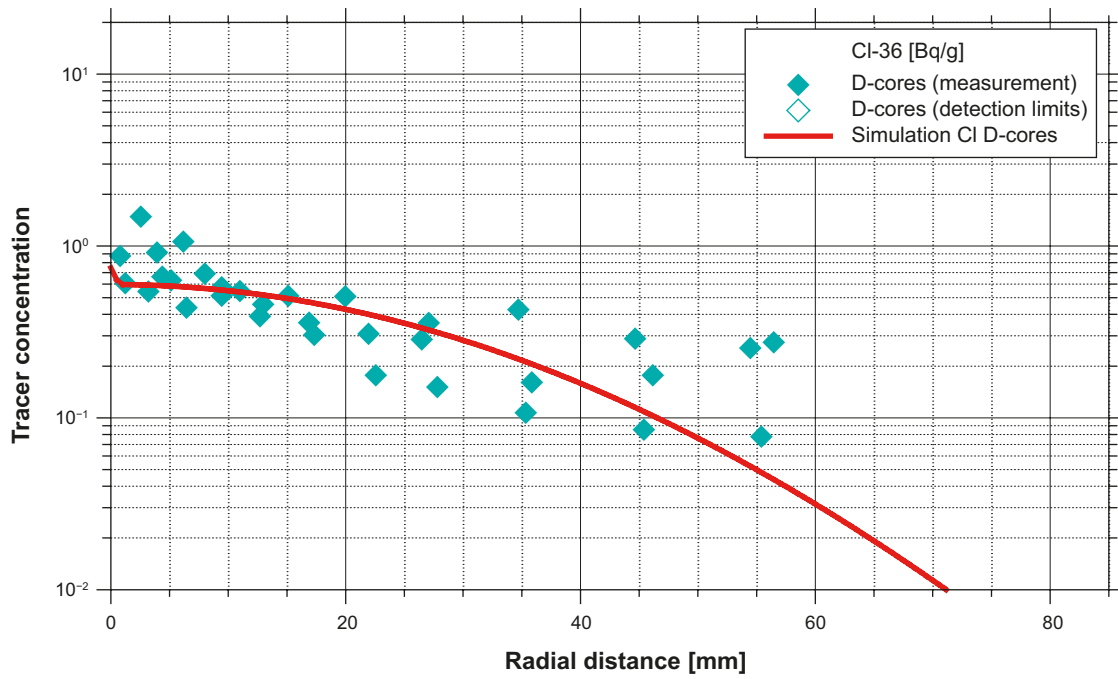| D-cores	$^{36}Cl^-$	$^{22}Na^+$	$^{137}Cs^+$	$^{133}Ba^{2+}$
Φ_{BDZ} [-]	0.001	0.001	0.001	0.001
τ^+_{BDZ} [-]	0.001	0.001	0.001	0.001
I_{BDZ} [mm]	1	1	1	1
Φ_{matrix} [-]	0.0008	0.004	0.004	0.004
τ^+_{matrix} [-]	0.005	0.4	0.4	0.4
m [-]	2	2	2	2

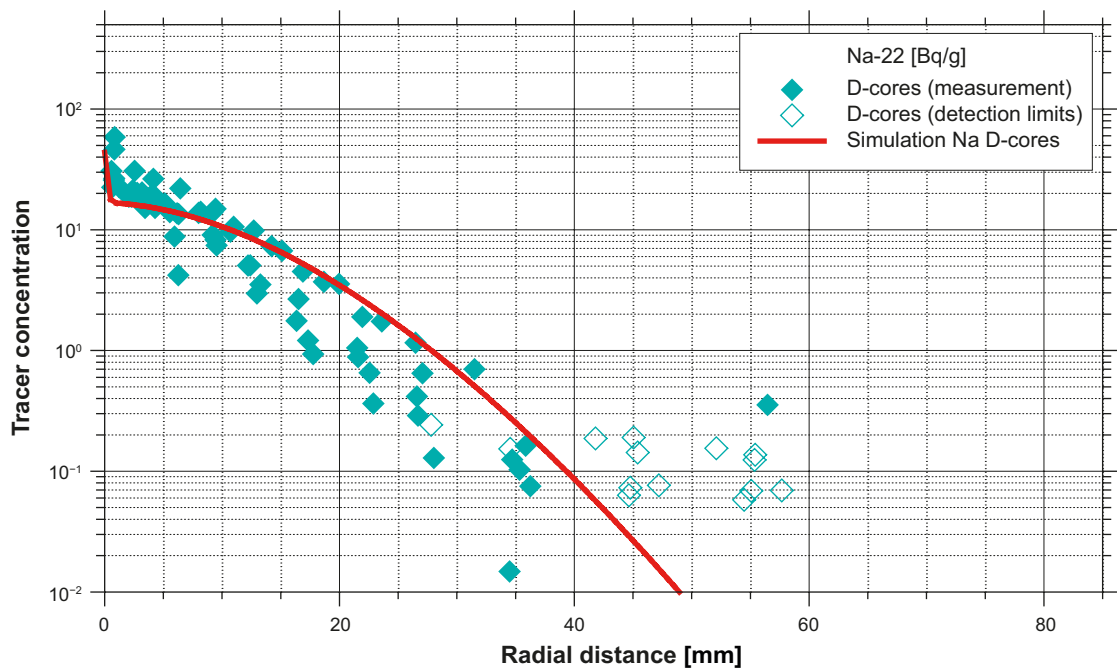**Figure 3-6.** *Fit of the two-zone model to the $^{36}Cl^-$-data set from the D-cores.*

Figure 3-7. *Fit of the two-zone model to the $^{22}Na^+$-data set from the D-cores.*

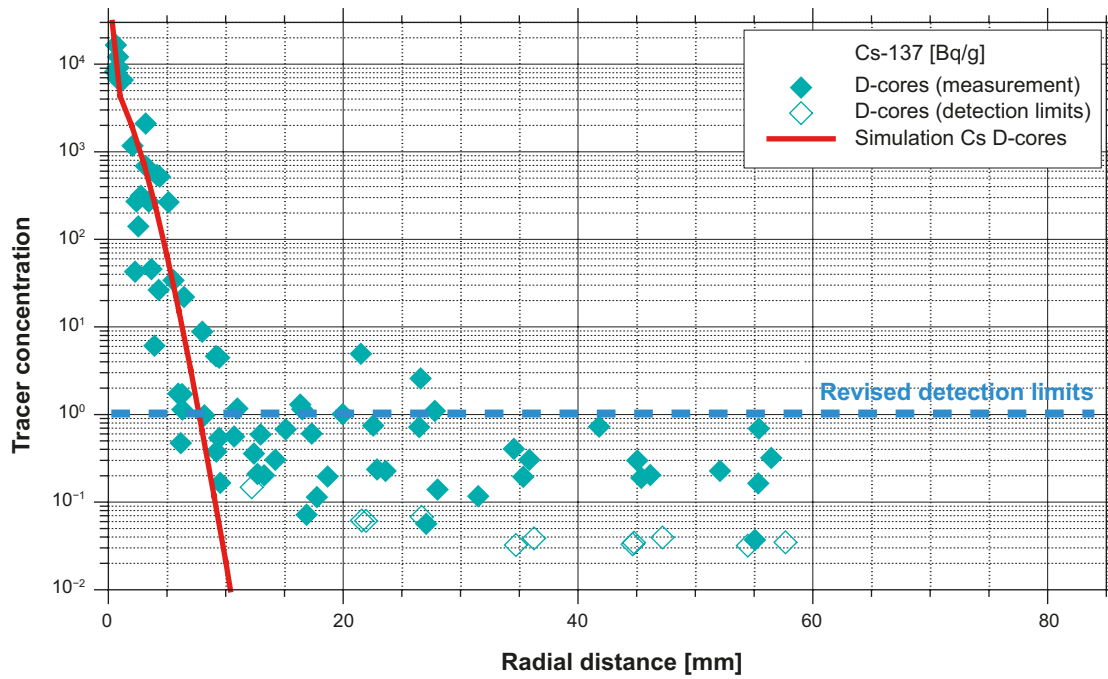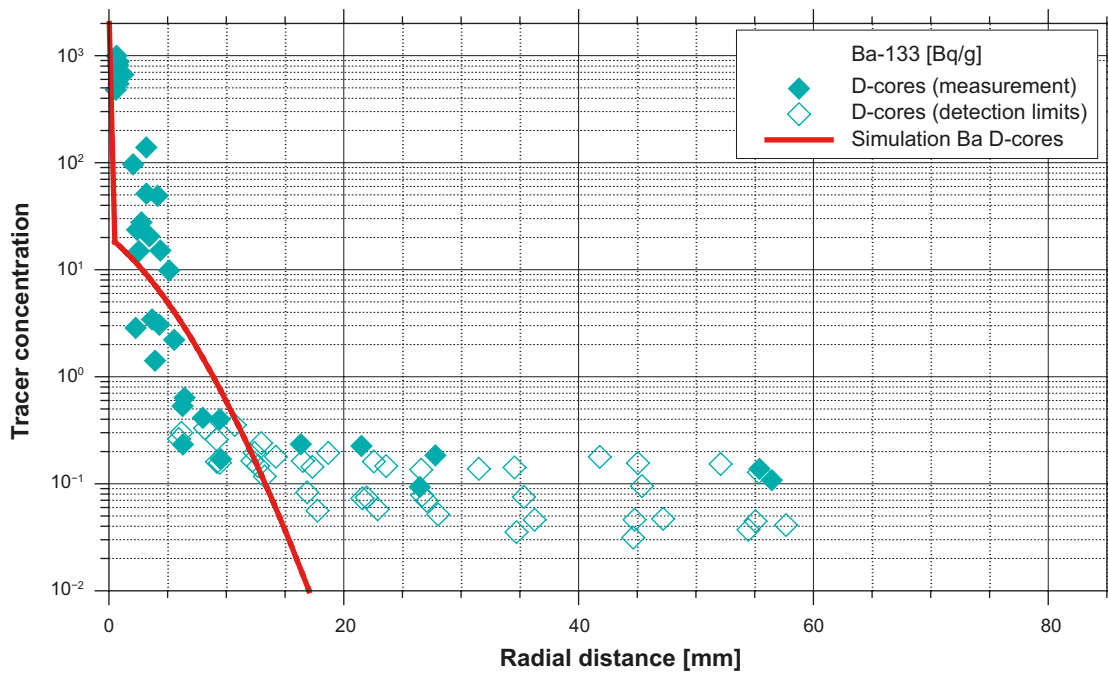**Figure 3-8.** *Fit of the two-zone model to the $^{137}Cs^+$-data set from the D-cores.*

Figure 3-9. *Fit of the two-zone model to the $^{133}Ba^{2+}$-data set from the D-cores.*

4 Summary and conclusions

The Long-Term Diffusion Experiment (LTDE) has been carried out at the Hard Rock Laboratory (HRL) Äspö in Sweden in order to check the concepts of diffusion and sorption of radioactive nuclides in crystalline rock. The test set-up was designed in such a way that 22 different solutes could enter the rock via a test borehole or from a controlled section of a natural fracture wall.

Tracer profiles were determined after the end of the test. They showed a peculiar shape, basically a steep gradient close to the rock surface followed by a subsequently much lower gradient without a significant transition zone. Task 9b of the Task Force on Groundwater Flow and Transport of Solutes (TF GWFTS) of the Svensk Kärnbränslehantering (SKB) had therefore become engaged in reproducing the curious concentration curves.

Initially, this had been considered to be a complex chemical problem, drawing the attention of GRS to a potential qualification of the referring options in d^3f++. However, despite the gathered expertise among the participants of Task 9b explanation attempts went into numerous entirely different directions. The focus of GRS thus shifted towards finding a plausible mechanism. A major attempt had been the co-organising of a workshop on the so-called "skin-effect". The results encouraged GRS to check the plausibility of a two-zone model with a disturbed zone close to the rock surface and the undisturbed matrix beyond that.

A preceding data analysis provided valuable insight into reliability of the data as well as into the general structure of granite:

- In some cases the detection limits for the tracers appear to be related to the subsample sizes as indicated in Figure 2-2.

- If the activity values are in the same range and show the same trend as the detection limits as in case of $^{226}Ra^{2+}$ the activity data becomes meaningless. Concentration values that lie at the detection limits or below must be considered to be at least comparatively badly known and should thus not be used for a comparison with model results.

- Only the activity data for $^{22}Na^+$, $^{36}Cl^-$, $^{137}Cs^+$, $^{57}Co^{2+}$, and $^{133}Ba^{2+}$ are entirely or at least partially relevant in that the data points lie clearly above the detection limits.

- Data for $^{36}Cl^-$ and $^{22}Na^+$ from the D-cores do not show the steep concentration gradient in the immediate vicinity of the former reservoir.

- Due to the different nature of the disturbed zones for A- and D-cores namely fracture coating and a BDZ, respectively, a principal difference is expected for A- and D-cores.

- There is much less data uncertainty within a drill core than scatter between the cores. This indicates considerable local variation of material properties in the matrix on the scale of the LTDE. Fitting model results to the data can therefore not be done as stringent as it had been hoped for.

As few parameters as possible were used to fit numerical results to the measurements. The fitting procedure was subject to several restrictions that followed from the approach of the two-zone model:

- The geometric parameters Φ and τ^+ for the undisturbed matrix should be the same for all eight models. A possible exception could be lower values for $^{36}Cl^-$ in case of anion exclusion. These would have to be the same for A- and D-cores, though.

- For the disturbed zone, these parameters should be equal for the A-cores as well as for the D-cores but may be different for A- and D-cores due to the different nature of the disturbed zone (fracture coating or BDZ).

- The same applies to the extension of the disturbed zone and the shape of the transition function for Φ and τ^+ across the disturbed zone.

Six parameters are thus required for each transport model. As four tracers are investigated here and since different models were used for the A- and for the D-cores, all in all eight models have been set up for the fitting procedure. The model parameters resulting from the fitting procedure are listed in Table 3-1 for the A-core models and in Table 3-2 for the D-core models.

All six models for the cations could be fit in such way that Φ_{matrix} and τ^+_{matrix} are the same (0.004 and 0.4, respectively). Moreover, the porosity derived for the cations as well as the tortuosity$^+$-value is reasonably close to expectations for the undisturbed matrix.

For $^{36}Cl^-$, however, both parameters are considerably lower but nevertheless the same for A- and D-cores (0.0008 and 0.005, respectively). This observation indicates that the anions experienced anion exclusion by very narrow pore channels, indeed. Unfortunately, this means also that $^{36}Cl^-$ cannot be taken as an ideal tracer for deriving the topological parameters of the pore space. The parameters for the cations thus could not be confirmed by the fitting exercise in step 1 as planned. However, the resulting parameters concerning the undisturbed matrix obey the first condition listed above.

The four parameters concerning the disturbed zone Φ_{BDZ}, τ^+_{BDZ}, l_{BDZ}, and m satisfy the second and the third condition listed above as well. They show different values for Φ_{BDZ} and τ^+_{BDZ} between the A-cores (0.003 and 0.0006, respectively) and the D-cores (0.001 and 0.001, respectively) as expected from the different nature of the disturbed zone. Noteworthy are these parameters also since they seem to be reduced in comparison to the ones for the undisturbed matrix.

A bit unexpected, though, is the observation that l_{BDZ} and m are the same for all eight models (1 mm and exponent 2). Additionally, it has to be conceded that the $^{36}Cl^-$-profile from the A-cores indicates rather a depth of 5 mm for the disturbed zone which is unique among the data sets investigated here. No explanation could be found for this observation.

By and large, the parameters derived from the fitting procedure explain the tracer profiles reasonably well, particularly considering that the tracer profiles for $^{36}Cl^-$ and $^{22}Na^+$ in the D-cores do not show the characteristic steep concentration gradient at the sample surface at all. At that, the results confirm the plausibility of the two-zone approach with a narrow disturbed zone and an undisturbed matrix. However, this cannot be mistaken for a proof of concept as there are many other explanations for the curious tracer profiles that may prove to viable as well. As long as the true reasons behind the strange tracer profiles are not known, correctness cannot be stated and the relevance for long-term safety cannot be evaluated.

What remains to be noted is certainly the surprisingly high degree of inhomogeneity among the drill cores that led to nice individual tracer profiles but a quite broad band when all data points were put together. It might be worthwhile to fit the curve parameters to each individual curve and to derive the uncertainty that is the consequence of the local inhomogeneity. Qualitatively, the data scatter between the different curves should also be taken as a warning to be careful if using a homogeneous model for transport phenomena in crystalline rock.

References

SKB's (Svensk Kärnbränslehantering AB) publications can be found at www.skb.com/publications.

Kröhn K-P, 2018. Hydraulic interaction of engineered and natural barriers – Task 8e of SKB. Summary report. FKZ 02 E 11213 (BMWi), GRS-431, Gesellschaft für Anlagen- und Reaktorsicherheit (GRS) mbH, Germany.

Kröhn K-P, Lanyon B (eds), 2018. Observations of hydraulic and transport „Skin effects". SKB Task Force Workshop Prague 2016. FKZ 02 E 11476A (BMWi), GRS-504, Gesellschaft für Anlagen- und Reaktorsicherheit (GRS) mbH, Germany.

Kull H (ed), Helmig R, Jacobs H, Jockwer N, Kröhn K-P, Zimmer U, 2002. Two-phase-flow experiment in the fractured crystalline rock of the Äspö Hard Rock laboratory. Final report. FKZ 02 E 9027 8 (BMFT), Report GRS-183, Gesellschaft für Anlagen- und Reaktorsicherheit (GRS) mbH, Germany.

Li Y-H, Gregory S, 1974. Diffusion of ions in sea water and in deep-sea sediments. Geochimica et Cosmochimica Acta 38, 703–714.

Löfgren M, Nilsson K, 2020. Task description of Task 9B – Modelling of LTDE-SD performed at Äspö HRL. Task 9 of SKB Task Force GWFTS – Increasing the realism in solute transport modelling based on the field experiments REPRO and LTDE-SD. SKB P-17-30, Svensk Kärnbränslehantering AB.

Nilsson K, Byegård J, Selnert E, Widestrand H, Höglund S, Gustafsson E, 2010. Äspö Hard Rock Laboratory. Long Term Sorption Diffusion Experiment (LTDE-SD). Results from rock sample analyses and modelling. SKB R-10-68, Svensk Kärnbränslehantering AB.

Widestrand H, Byegård J, Selnert E, Skålberg M, Höglund S, Gustafsson E, 2010a. Long Term Sorption Diffusion Experiment (LTDE-SD). Supporting laboratory program. Sorption diffusion experiments and rock material characterisation. With supple-ment of adsorption studies on intact rock samples from the Forsmark and Laxemar site investigations. SKB R-10-66, Svensk Kärnbränslehantering AB.

Widestrand H, Byegård J, Nilsson K, Höglund S, Gustafsson E, Kronberg M, 2010b. Long Term Sorption Diffusion Experiment (LTDE-SD). Performance of main in situ experiment and results from water phase measurements. SKB R-10-67, Svensk Kärnbränslehantering AB.

Tracer data

Data for modelling LTDE-SD

Table A1-1. Grouping of tracer materials according to sorption mechanisms.

Ion	Appearance	An-/cationic	Comments
Non-sorbing			
$^{36}Cl^-$	Predominately as anionic Cl^-	√	Anion exclusion?
Ion exchange			
$^{22}Na^+$	Predominately as cationic Na^+	√	
$^{133}Ba^{2+}$	?		
$^{137}Cs^+$	Predominately in cationic form	√	
$^{226}Ra^{2+}$	Totally as cationic Ra^{2+}	√	
Surface complexation			
$^{57}Co^{2+}$	Both anionic and cationic	(√)	
$^{63}Ni^{2+}$	Predominately as cationic Ni^{2+}	√	
$^{109}Cd^{2+}$	Only 3 % as cationic Cd^{2+}	√	Heavy metal
$^{110m}Ag^+$	Only 4 % as non-charged $AgCl$		
$^{153}Gd^{3+}$	Complex speciation chemistry		
Electrochemical reduction dependent			
$^{237}Np^{3+}$	Sensitive to the redox potential		

Note the comment in Widestrand et al. (2010a) with respect to elements sorbing by surface complexation: "These elements show a tendency not to reach sorption equilibrium after 186 days …".

Table A1-2. Tracer half-lifes.

Ion	Half-life
$^{36}Cl^-$	301 000 a
$^{22}Na^+$	2.602 a
$^{133}Ba^{2+}$	10.51 a
$^{137}Cs^+$	30.17 a
$^{226}Ra^{2+}$	1 602 a
$^{57}Co^{2+}$	271.79 d
$^{63}Ni^{2+}$	100.1 a
$^{109}Cd^{2+}$	462.6 d
$^{110m}Ag^+$	249.79 d
$^{153}Gd^{3+}$	241.6 d
$^{237}Np^{3+}$	2.144×10^6 a

Table A1-3. K_d-values evaluated in batch experiments; from Widestrand et al. (2010a).

Sorted by sorption categories		Sorted by K_d-values	
Ion	**K_d [m³/kg]**	**Ion**	**K_d [m³/kg]**
$^{36}Cl^-$	~ 0	$^{36}Cl^-$	~ 0
$^{22}Na^+$	2.90×10^{-04}	$^{22}Na^+$	2.90×10^{-04}
$^{133}Ba^{2+}$	2.10×10^{-03}	$^{237}Np^{3+}$	8.20×10^{-04}
$^{137}Cs^+$	2.20×10^{-02}	$^{133}Ba^{2+}$	2.10×10^{-03}
$^{226}Ra^{2+}$	7.50×10^{-03}	$^{109}Cd^{2+}$	5.07×10^{-03}
$^{57}Co^{2+}$	4.97×10^{-02}	$^{226}Ra^{2+}$	7.50×10^{-03}
$^{63}Ni^{2+}$	1.54×10^{-02}	$^{63}Ni^{2+}$	1.54×10^{-02}
$^{109}Cd^{2+}$	5.07×10^{-03}	$^{137}Cs^+$	2.20×10^{-02}
$^{110m}Ag^+$		$^{57}Co^{2+}$	4.97×10^{-02}
$^{153}Gd^{3+}$		$^{110m}Ag^+$	
$^{237}Np^{3+}$	8.20×10^{-04}	$^{153}Gd^{3+}$	

Data for diffusion coefficients had to be compiled and processed. Details are given right after Table A1-4.

Table A1-4. Diffusion coefficients.

Ion	appearance	an-/cationic	Self-diffusion coefficient at 15 °C [10^{-10} m²/s]
$^{36}Cl^-$	Predominately as anionic Cl^-	√	15.8
$^{22}Na^+$	Predominately as cationic Na^+	√	10.3
$^{133}Ba^{2+}$	?		6.5
$^{137}Cs^+$	Predominately in cationic form	√	16.4
$^{226}Ra^{2+}$	Totally as cationic Ra^{2+}	√	6.8
$^{57}Co^{2+}$	Both anionic and cationic	(√)	5.2
$^{63}Ni^{2+}$	Predominately as cationic Ni^{2+}	√	5.3
$^{109}Cd^{2+}$	Only 3 % as cationic Cd^{2+}	√	5.5
$^{110m}Ag^+$	Only 4 % as non-charged AgCl		13.0
$^{153}Gd^{3+}$	Complex speciation chemistry		
$^{237}Np^{3+}$	Sensitive to the redox potential		

Starting point for deriving the diffusion coefficients is the Nernst expression (Robinson and Stokes 1959, cited in Li and Gregory 1974):

$$D_j^0 = \frac{RT\,\lambda_j}{\left|Z_j\right|F^2} \tag{A1-1}$$

D_j^0 –   limiting tracer- or self-diffusion coefficient of ion j

λ_j^0 –   limiting equivalent conductivity of ion j

Z_j –   absolute value of charge of ion j

R –   gas constant

T –   absolute temperature

F –   Faraday constant

An estimation of λ_j^0 at 25 °C can be given by an empirical formula after Nigrini (1970, cited in Li and Gregory 1974) (for temperatures between 60° and 300 °C another formula is proposed by Nigrini (1970, cited in Li and Gregory 1974)):

$$\lambda_j^0 = 10.56 + 90.72 \log Z_j + 42.95 \frac{\gamma_j}{Z_j} \tag{A1-2}$$

γ_j – crystal ionic radius of ion j

Stokes-Einstein relation for self-diffusion of water reads

$$\left(\frac{D^0 \eta^0}{T} \right)_{T_1} = \left(\frac{D^0 \eta^0}{T} \right)_{T_2} \tag{A1-3}$$

η^0 – viscosity of water

and has been shown to hold for a temperature range of 0–100 °C (Simpson and Carr 1958, cited in Li and Gregory 1974). For ions „diffusing slower than the fluoride ion", this equation holds also „fairly well in the temperature range relevant to the ocean" (Li and Gregory 1974). For faster diffusing ions another equation is proposed by Li and Gregory (1974):

$$\left(D^0 \eta^0 \right)_{T_1} = \left(D^0 \eta^0 \right)_{T_2} \tag{A1-4}$$

The diffusion coefficients as a function of ionic potential at 25 °C are depicted in Figure A1-1 and compiled in Table A1-5. The higher the ionic potential, the larger is the hydration shell, and the lower is the diffusion coefficient. The data given in Table A1-4 are linearly interpolated from the data in Table A1-5 assuming an ambient temperature of 15 °C. Note that the diffusion coefficients differ by less than a factor of 4.

Table A1-5. Diffusion coefficients after Li and Gregory (1974).

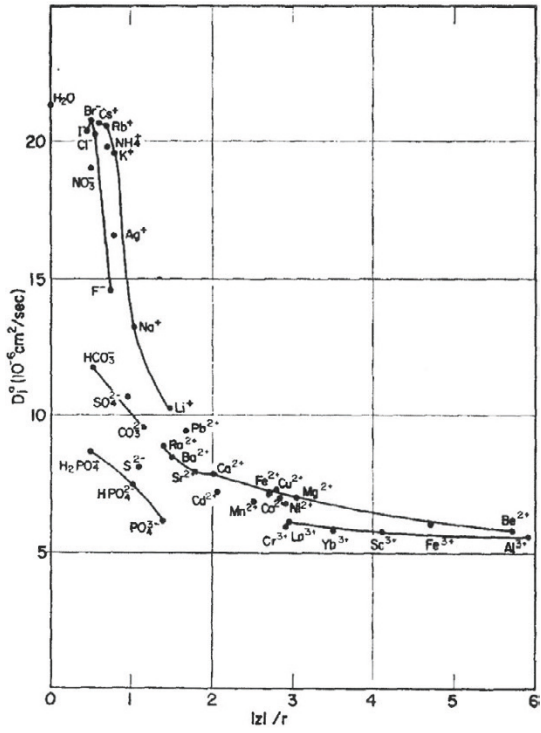| Ion	Self-diffusion coefficient [10^{-10} m²/s]		
	0 °C	18 °C	25 °C
$^{36}Cl^-$	10.1	17.1	20.3
$^{22}Na^+$	6.27	11.3	13.3
$^{137}Cs^+$	10.6	17.7	20.7
$^{133}Ba^{2+}$	4.04	7.13	8.48
$^{226}Ra^{2+}$	4.02	7.45	9.89
$^{109}Cd^{2+}$	3.41	6.03	7.17
$^{237}Np^{3+}$			
$^{57}Co^{2+}$	3.41	5.72	6.99
$^{63}Ni^{2+}$	3.11	5.81	6.79
$^{110}Ag^+$	8.5	14	16.6
$^{153}Gd^{3+}$			
^{19}F		12.1	14.6

Figure A1-1. *Tracer- or self-diffusion coefficient as a function of ionic potential at 25 °C; from Li and Gregory (1974).*

Experimental data during the tests

The tracer concentration in the injection volume for the solution containing the tracers was monitored over time. The data are visualized in Figure A2-1. Note that the units in which the concentrations for the tracers are given vary.

While some of the tracer concentrations are more or less constant over the whole active period of the experiment, some show a dramatic decrease. In Table A2-1 the tracers together with minimum and maximum concentration value are listed. Looking at the ratio between maximum and minimum concentration, the tracers can be divided into 3 groups: ratio < 2 ($^{36}Cl^-$, $^{22}Na^+$, $^{133}Ba^{2+}$, $^{237}Np^{3+}$), ratio between 2 and 5 ($^{226}Ra^{2+}$, $^{137}Cs^+$, $^{63}Ni^{2+}$, $^{109}Cd^{2+}$), and ratio > 100 ($^{110m}Ag^+$, $^{57}Co^{2+}$, $^{153}Gd^{3+}$). The temporal development of concentrations in the reservoir is depicted in Figure A2-2 where the activity is plotted over time in a logarithmic and a linear scale.

While the tracers from the first group qualify for approximating the initial value in the reservoir by a constant (with a view to boundary conditions of a numerical model) it appears to be less justifiable in case of the second and to be certainly not appropriate for the third group. However, a significant loss in concentration can be observed over the first ten days. Therefore also the concentration after this time and the related ratio are listed in Table A2-1. These ratios are significantly smaller and should allow for using these reduced values as a constant boundary condition in case of the second group of tracers. But a large error is possibly related to applying this procedure to the third group since a large amount of tracer would be lost in the numerical model.

Table A2-1. Characteristic data on tracer concentrations in the injection volume.

| Ion	Maximum concentration	Minimum concentration	Ratio	Concentration after 10 days	Ratio	Unit
$^{36}Cl^-$	5350	4980	1.1	5009	1.0	Bq/mL
$^{22}Na^+$	3200	2600	1.2	3025	1.2	Bq/mL
$^{133}Ba^{2+}$	1450	960	1.5	1220	1.3	Bq/mL
$^{137}Cs^+$	7070	2680	2.6	4360	1.7	Bq/mL
$^{226}Ra^{2+}$	103	51.3	2.0	70.85	1.4	Bq/g
$^{57}Co^{2+}$	13600	87.0	156.3	210.7	2.4	Bq/mL
$^{63}Ni^{2+}$	22200	7900	2.8	13635	1.7	Bq/mL
$^{109}Cd^{2+}$	21524	4310	5.0	8312	1.9	Bq/g
$^{110m}Ag^+$	235	1.98	118.7	-	-	Bq/g
$^{153}Gd^{3+}$	3084	11.3	272.0	18.88	1.7	Bq/g
$^{237}Np^{3+}$	272	168	1.6	218.3	1.3	ng/g
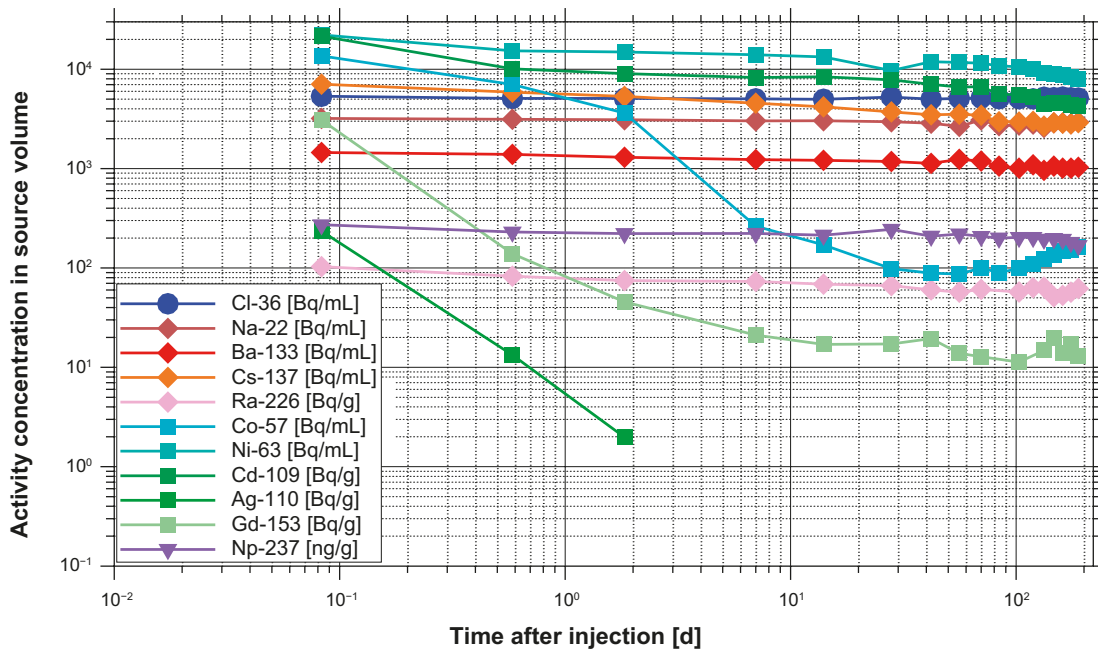
Figure A2-1. Tracer concentrations in the injection volume over time.
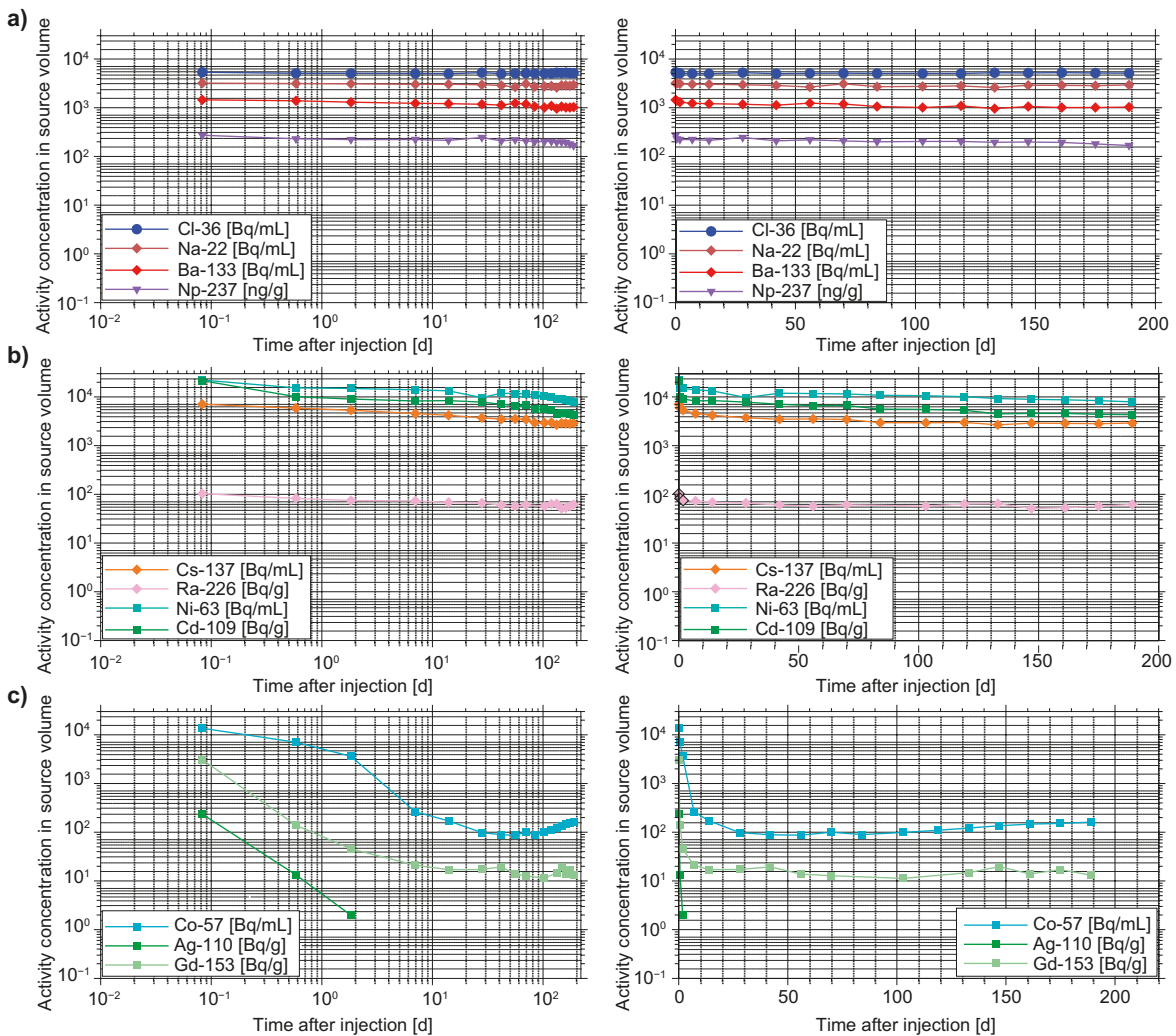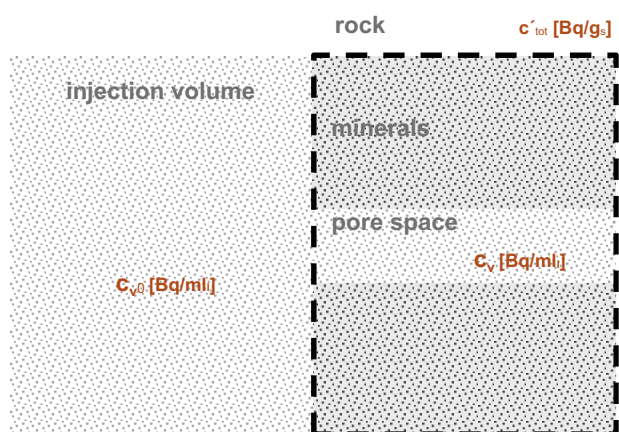

Figure A2-2. Tracer concentrations in the injection volume over time sorted after ratio; a) ratio < 2; b) ratio between 2 and 5; c) ratio > 100; time on the x-axis in a logarithmic scale on the left hand side, linear on the right hand side.

Conversion of tracer concentration units

While the tracer concentration in the injection volume is measured in Becquerel per volume of solution or per mass of solution, the concentration profiles in the samples are given in Becquerel per mass of rock. This is a practical unit as determination of tracer mass is done on the rock sample. Input for the numerical transport model can only be the monitored solution based concentrations. As a result the model provides the tracer concentrations related to the groundwater in the pore space of the rock. In order to compare model results with the measurements, the groundwater related concentration must be transformed into a rock related concentration. This situation is sketched in Figure A3-1 together with the symbols for the different concentrations. In terms of the task is to derive c'_{tot} from the numerically calculated concentration c_v in the rock.

c_{v0} – tracer concentration of the solution in the injection volume [Bq/ml]

c'_{tot} – activity measured in the rock after termination of the test [Bq/g_rock]

c_v – tracer concentration of the solution in the rock [Bq/ml]

Figure A3-1. *Relevant concentrations in the experiment.*

The basic relation between solute concentration and sorbed solute mass reads

$$c' = K_d \, \rho_l \, c \qquad\qquad (A3\text{-}1)$$

c — solute concentration related to mass of solution $[g_c/g_l]$

ρ_l — solution density $[g_l/ml_l]$

K_d — distribution coefficient $[ml_l/g\_rock]$

c' — solute concentration related to solid mass $[g_c/g\_rock]$

The distribution coefficient in (A3-1) is defined as

$$K_d = \frac{c'}{c_v} \qquad\qquad (A3\text{-}2)$$

c_v — solute concentration related to the volume of the solution $[g_c/ml_l]$

with

$$c_v = \rho_l \, c \qquad\qquad (A3\text{-}3)$$

The total activity as measured in the laboratory is the sum of solute in the water and adsorbed solute mass. While the sorbed mass concentration c' is already given in [Bq/g_rock], the unit for the tracer concentration c_v still in the solution must be transformed to the same dimensions. For this purpose, c_v is multiplied by the porosity in order to relate the solute mass to the bulk volume of the rock and then divided by the bulk rock density to relate the resulting expression to the rock mass:

$$c'_v = c_v \frac{\Phi}{\rho_s} \qquad\qquad (A3\text{-}4)$$

c'_v — equivalent sorbed solute mass $[g_c/g_s]$

ρ_s — rock bulk density $[g_s/ml_s]$

Φ — porosity $[ml_l/ml_s]$

The total activity is then calculated as

$$c'_{tot} = c' + c'_v \qquad\qquad (A3\text{-}5)$$

which can be expressed as a function of the solute concentration c_v with the help of Equation (A3-2) and (A3-4) as

$$c'_{tot} = c_v \left(K_d + \frac{\Phi}{\rho_s} \right) \qquad\qquad (A3\text{-}6)$$

Explanation of indices

c — solute

l — solution (liquid)

s — solid

Experimental data after the tests

The activity data of the determined profiles for the drill cores that were provided with the task description included many entries like "< x". These entries were interpreted as a detection limit for a specific subsample. The detection limits thus formed a distribution by themselves. Evaluation of these distributions alone as well as investigating their relation to the activity distributions proved to be quite revealing.

A characteristic example is given by the data for $^{226}Ra^{2+}$. Figure A4-1 shows the detection limits for $^{226}Ra^{2+}$ which seem – on a closer look – to form sections at different levels. In Figure A4-2 a dashed line is added to visualise the levels. Only in the first 5 mm there might be rather a gradient than a level. The subsample sizes are indicated as well by short vertical blue lines. The long vertical red lines, by contrast, separate sections of different subsample sizes showing clearly that the detection limits are correlated with the sample sizes. Similar observations even if not always as conclusive as in the case of $^{226}Ra^{2+}$ were made in case of the other tracers as well.
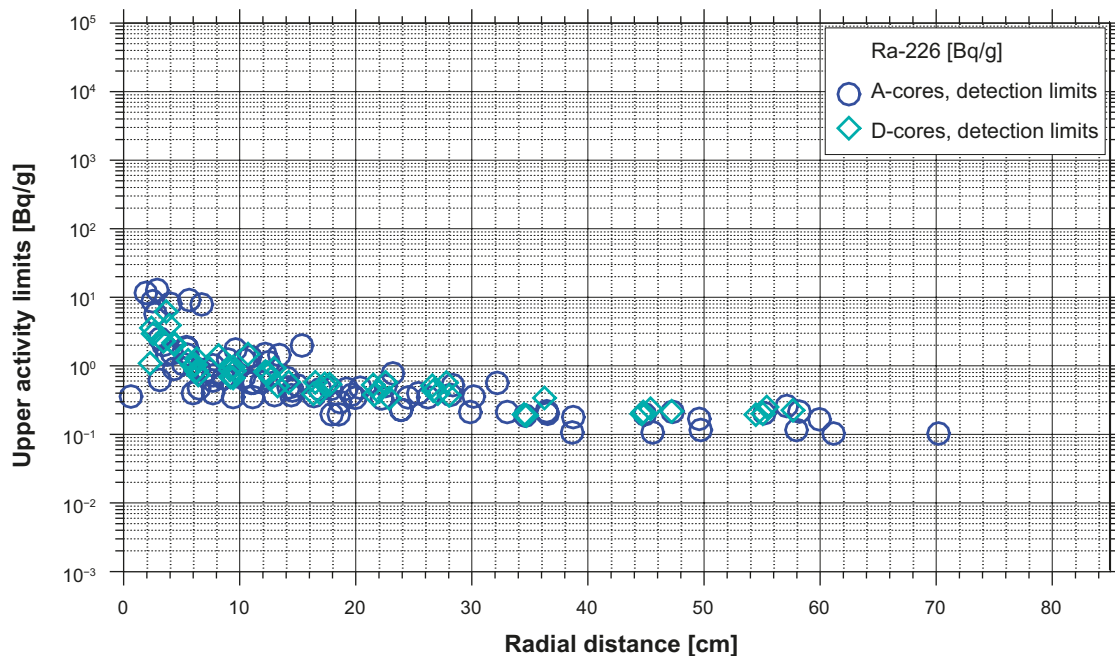
Figure A4-1. *Detection limits for $^{226}Ra^{2+}$ from A- and D-cores.*
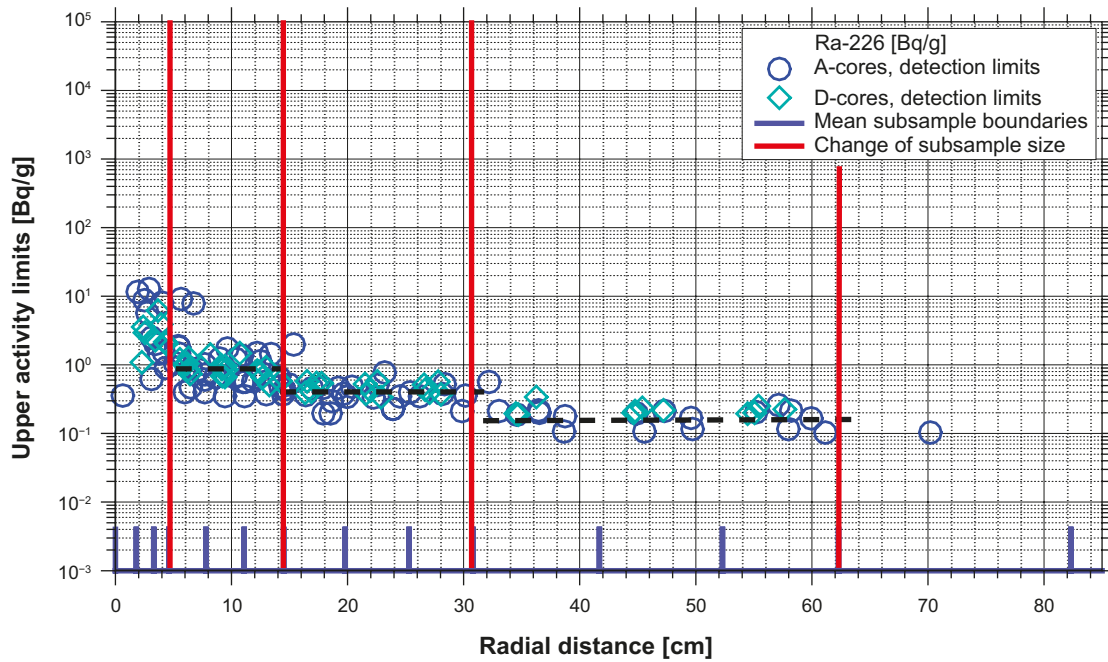
Figure A4-2. *Detection limits for $^{226}Ra^{2+}$ from A- and D-cores and subsample sizes.*

The relation of detection limits and sample sizes cannot come as a total surprise. It proves to become important, though, in the comparison of activity data and detection limits. Exemplarily, the activity data for $^{226}Ra^{2+}$ together with the related detection limits are shown in Figure A4-3. In this case there is no difference between data and detection limits beyond a depth of 2.5 mm into the drill core. Consequently, the activity data shows a certain drop in level at about 30 mm which coincides with the drop of the detection limits and the increase in sample size. Interpretation of activity data thus requires in general close inspection of the relation to the detection limits.
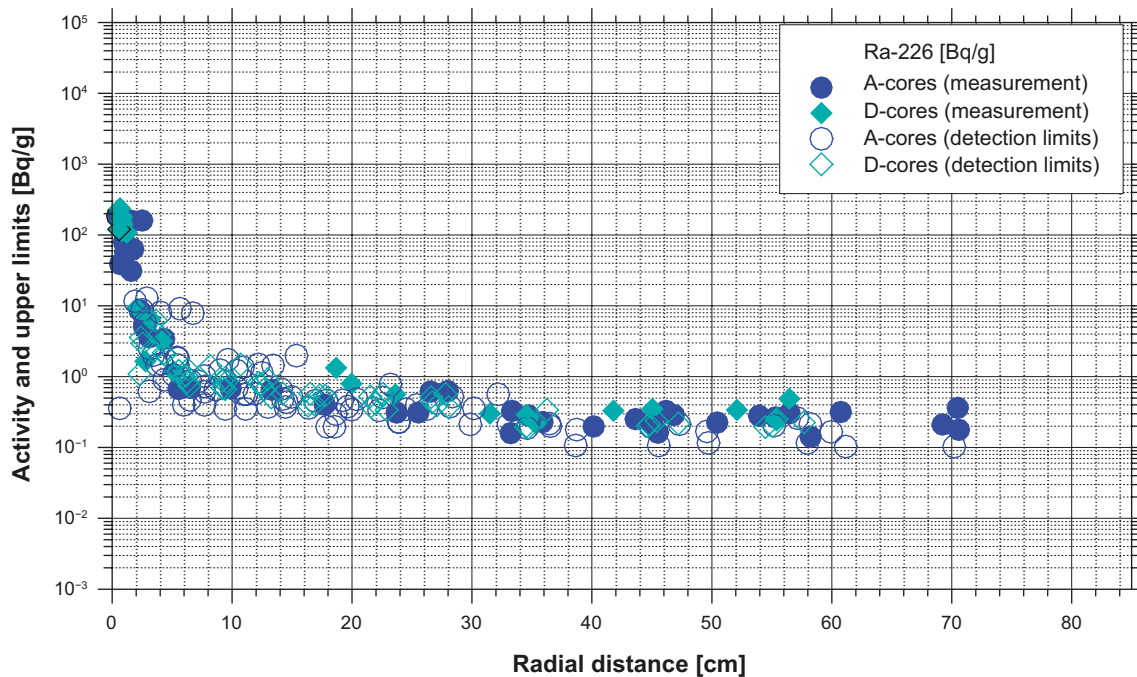
Figure A4-3. *Activity data and detection limits for $^{226}Ra^{2+}$ from A- and D-cores.*

All available activity data and detection limits were thus compared for all tracers that are relevant for Task 9b. In general, all tracer data are clearly above the detection limits within the first few millimetres into the drill core. However, only few tracer data proved to be significant beyond this margin. The comparison allowed for discriminating four groups of tracers (examples for each group are given in Figure A4-4):

– (1) Data points clearly above the cloud of detection limits (^{22}Na$^+$, ^{36}Cl$^-$, ^{137}Cs$^+$).

– (2) Data points "swimming" on top of the cloud of detection limits (^{57}Co^{2+}, ^{133}Ba^{2+}).

– (3) Data points inside the cloud of detection limits (^{109}Cd^{2+}, ^{110m}Ag$^+$, ^{153}Gd^{3+}, ^{226}Ra^{2+}).

– (4) Data points just for the first few millimetres (^{63}Ni^{2+}, ^{237}Np^{3+}).

It appears that only data from group (1) is entirely and only data from group (2) at least partly reliable and useful. Therefore, only the tracers ^{22}Na$^+$, ^{36}Cl$^-$, ^{137}Cs$^+$, and ^{133}Ba^{2+} will be addressed further on. Work on ^{57}Co^{2+} was dropped due to time limitations.
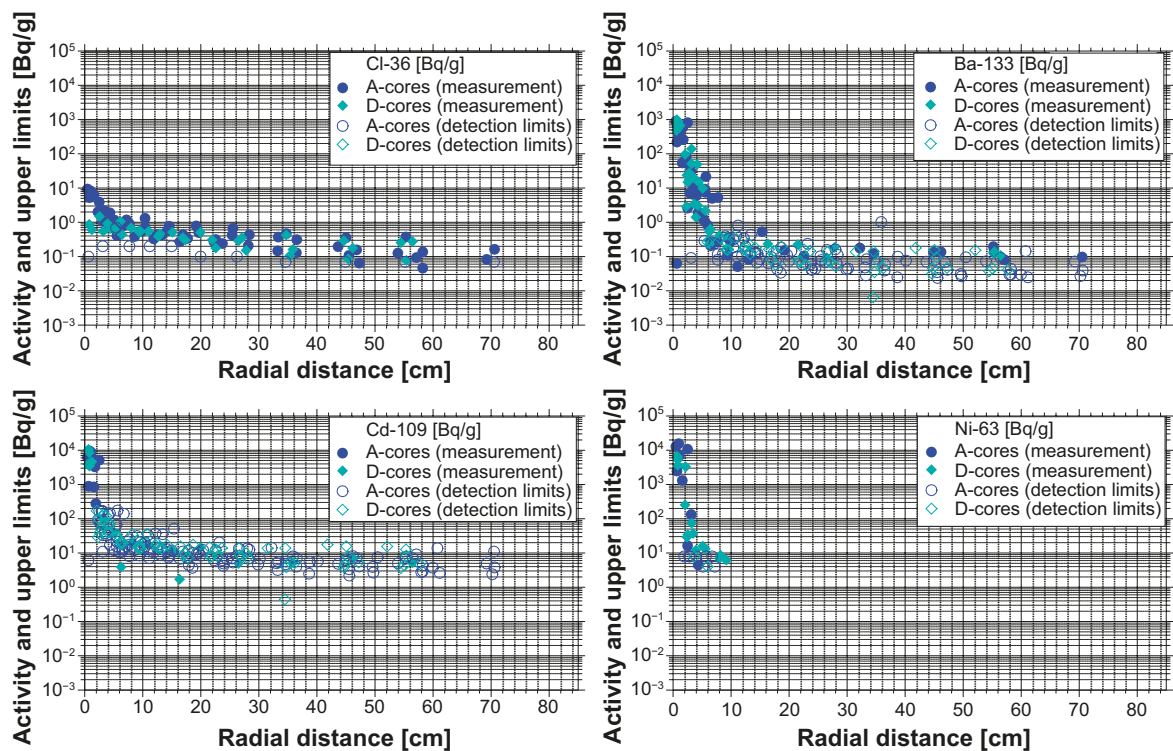
Figure A4-4. Activity and detection limits; groups (1) to (4) from top left to bottom right.

Separating the data for the A-cores from the data for the D-cores reveals a striking difference in the concentration distributions for $^{36}Cl^-$ and $^{22}Na^+$ as illustrated in Figure A4-5 to Figure A4-8. While most concentration distributions show a knee at about 5 mm this is not the case for $^{36}Cl^-$ and $^{22}Na^+$-data from the D-cores. There is no curious change in the profiles and the boundary concentration is considerably lower in case of $^{36}Cl^-$ and noticeably lower in case of $^{22}Na^+$. This observation alone seems to call for different models for A- and D-cores. Additionally, it should be kept in mind that the surfaces of the A-cores are in principle different from those of the D-cores as they show a fracture coating while the surface of the D-cores may have been influenced by a borehole disturbed zone (BDZ). Be that as it may, the matrix parameters for A- and D-cores should nevertheless be the same and relate basically to undisturbed conditions.
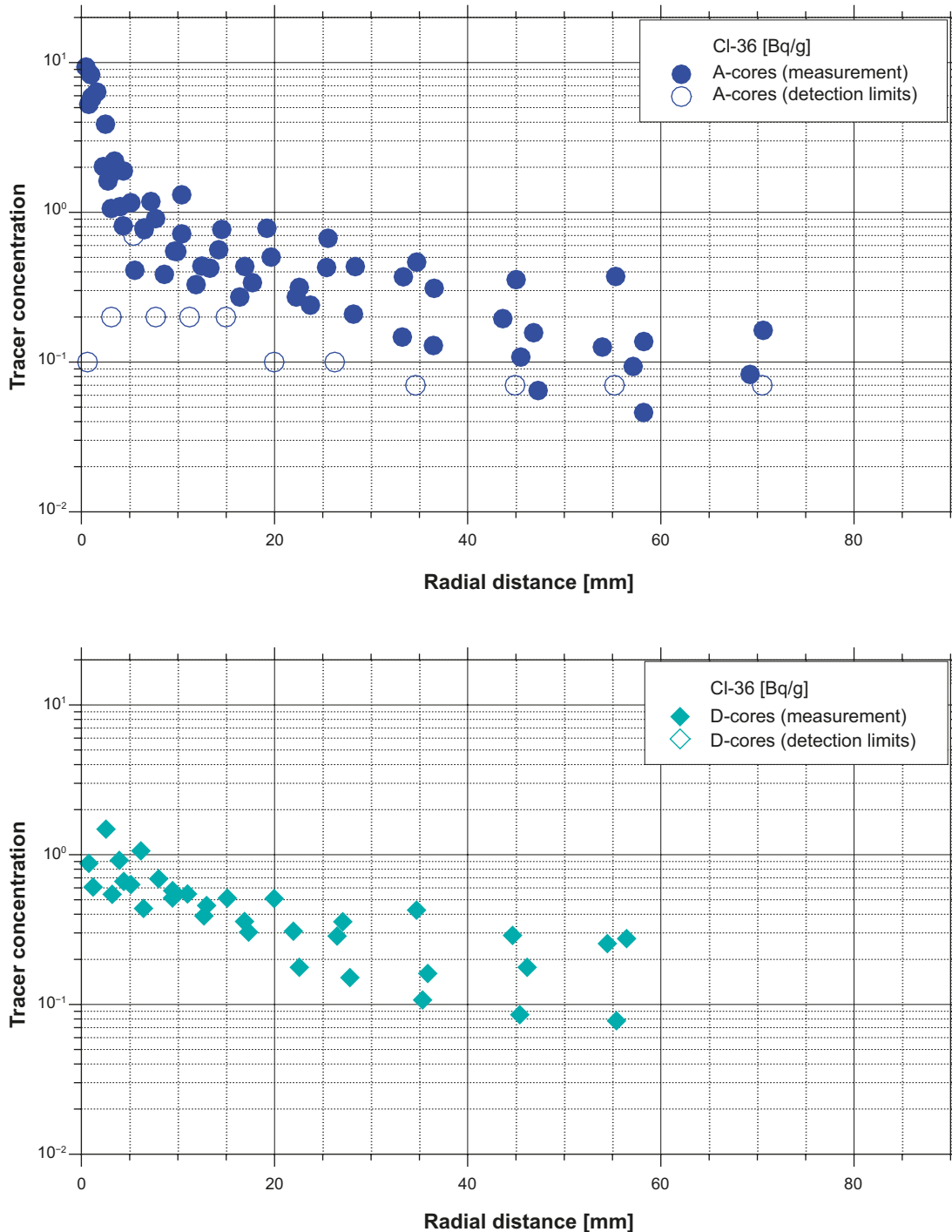
Figure A4-5. *Activity and detection limits for $^{36}Cl^-$; A-cores (top) and D-cores (bottom).*
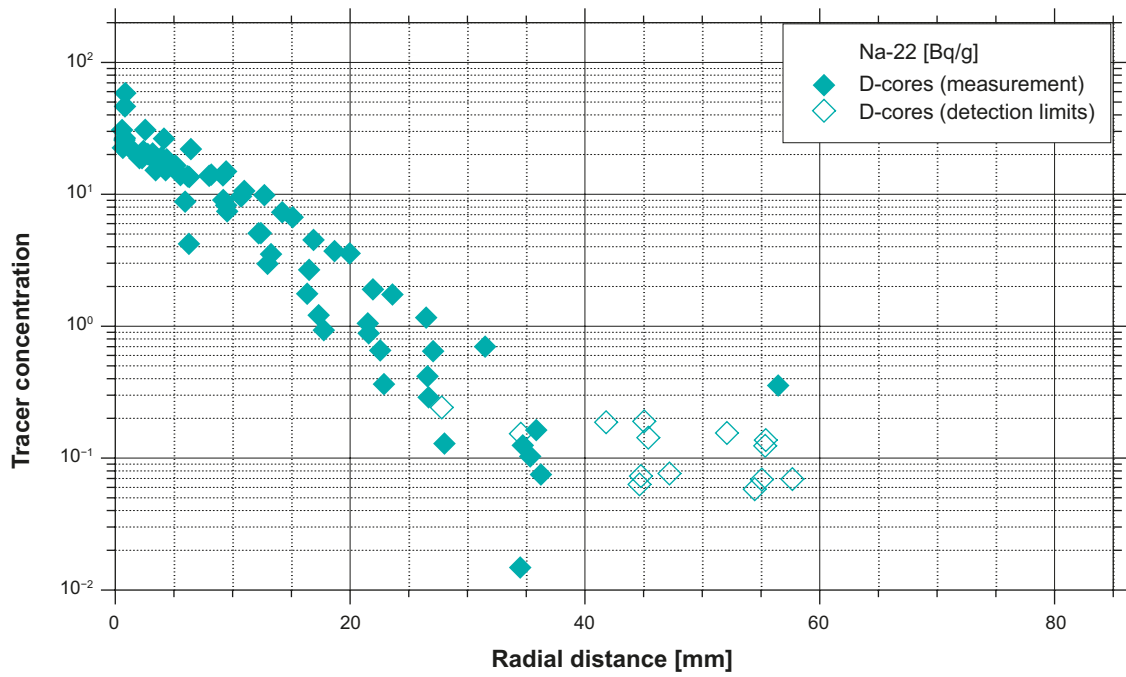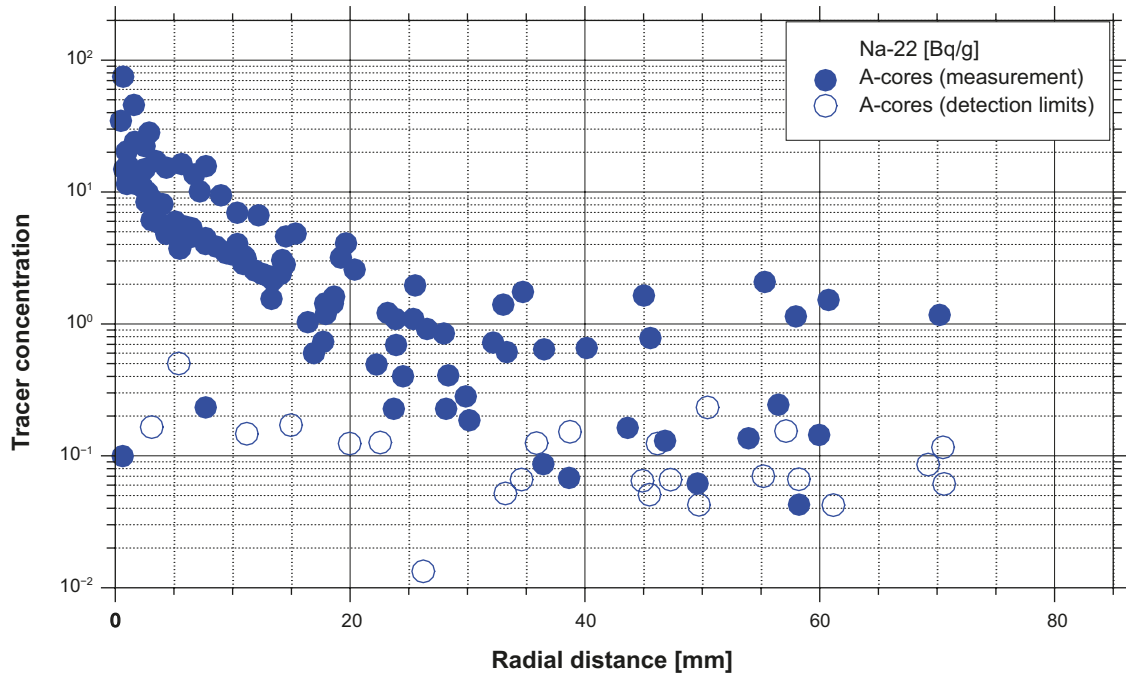
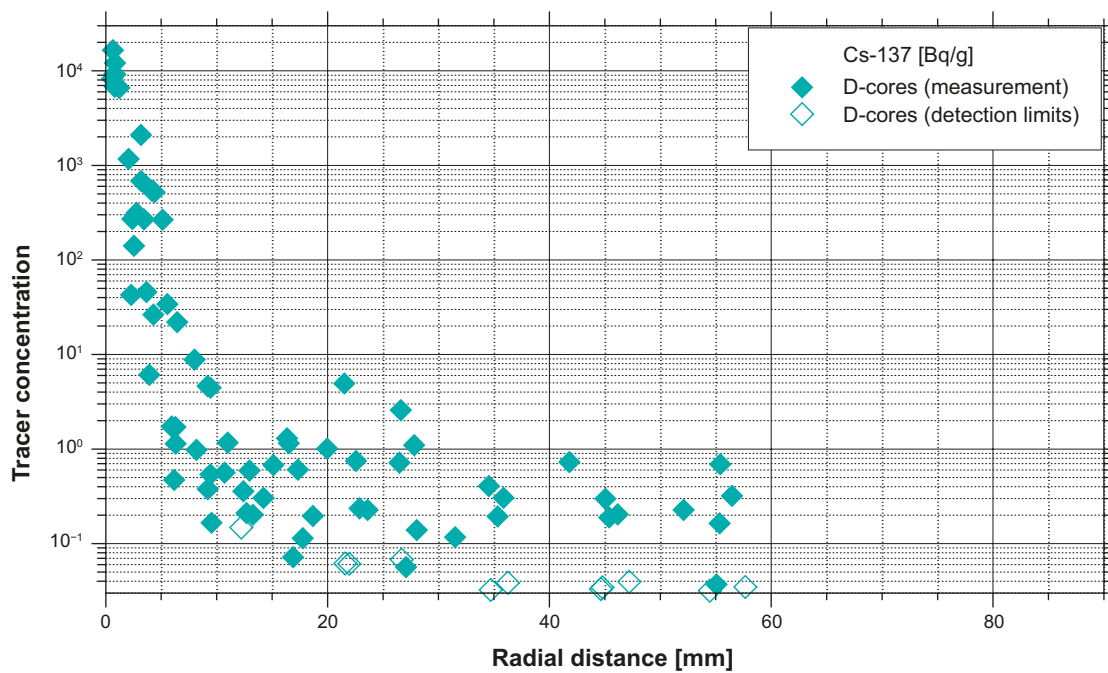**Figure A4-6.** *Activity and detection limits for $^{22}Na^+$; A-cores (top) and D-cores (bottom).*
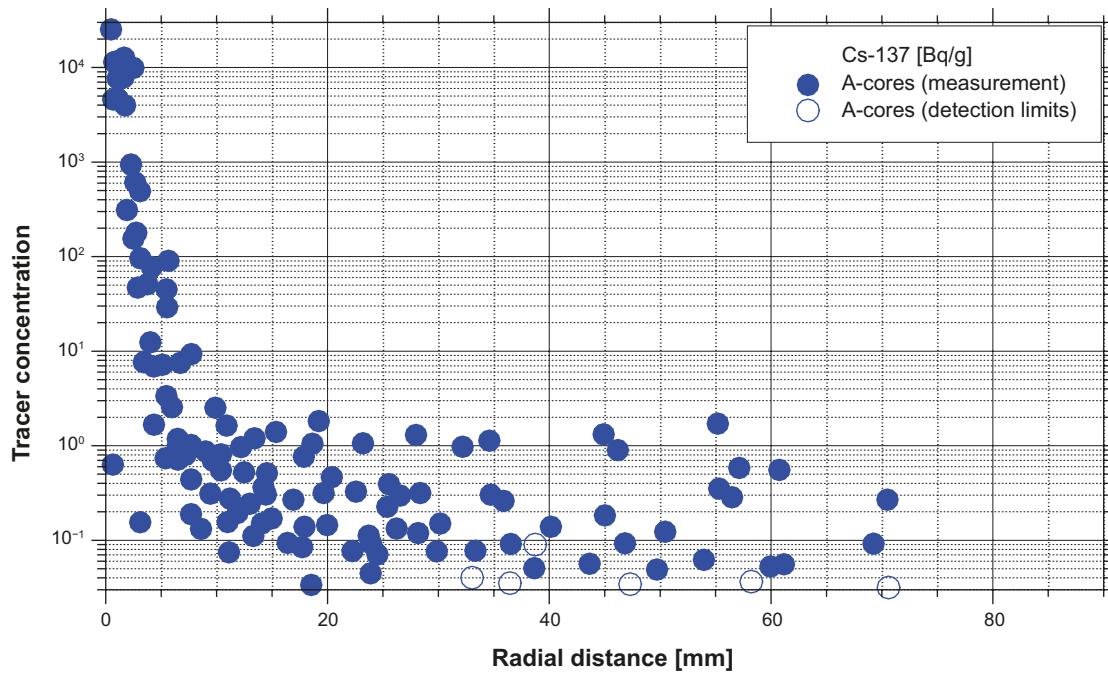
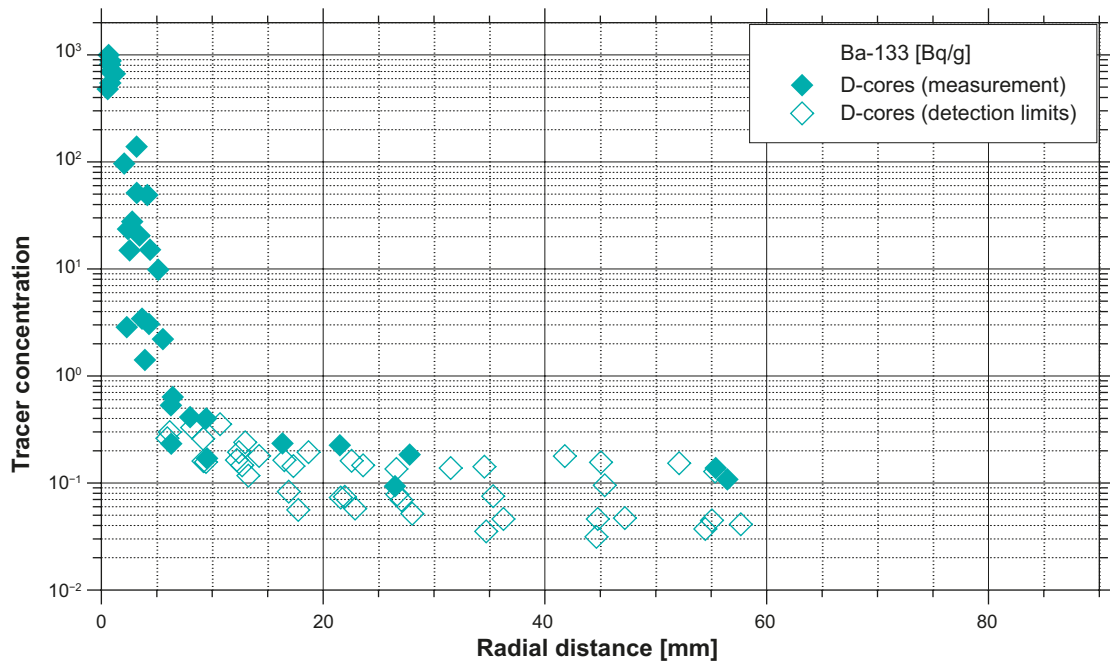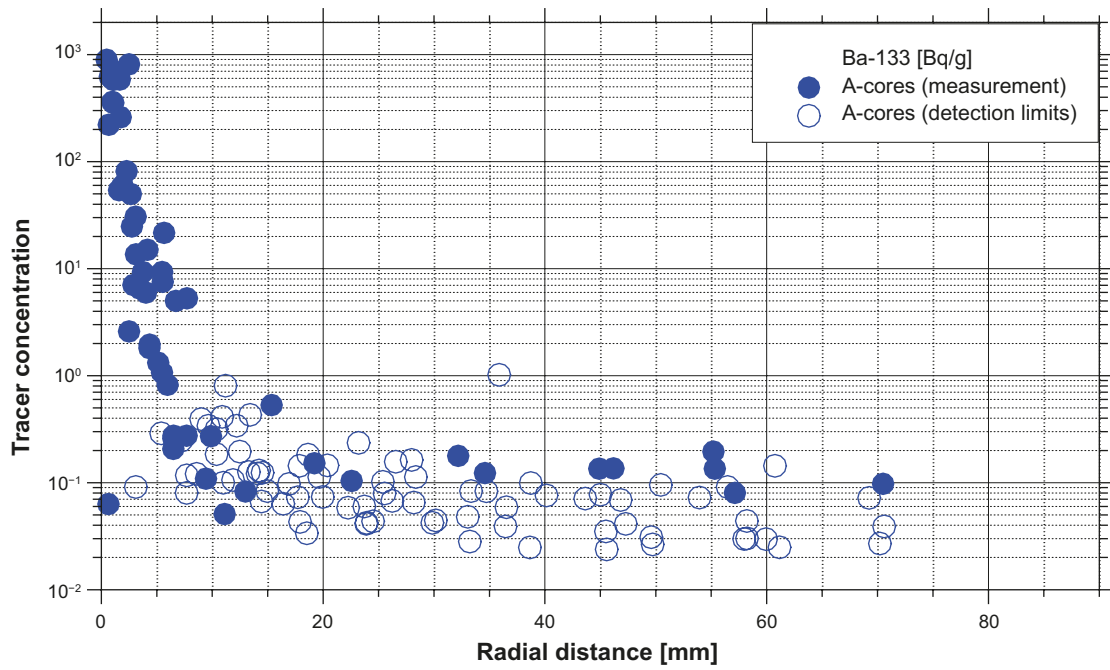**Figure A4-7.** *Activity and detection limits for $^{137}Cs^+$; A-cores (top) and D-cores (bottom).*

Figure A4-8. *Activity and detection limits for $^{133}Ba^{2+}$; A-cores (top) and D-cores (bottom).*

Examining Figure A4-5 to Figure A4-8 more closely, an interesting visualisation artefact has been discovered. Looking for instance at the ^{36}Cl$^-$-data in Figure A4-5, the data for both core types (A and D) have a comparatively broad bandwidth thereby provoking the impression of a large uncertainty in the individual data points. However, Figure A4-9 shows the same data as Figure A4-5 but the data from the different drill cores are marked with different colours. This results in the quite different impression that the curves from specific drill cores show quite clear trends but the trends differ from each other, in other words, there is much less data scatter within a drill core than between the cores. This is illustrated by Figure A4-10 where the coloured symbols are connected with thick lines of the same colour. Apparently, there is already considerable local variation of material properties in the matrix on the scale of the LTDE.
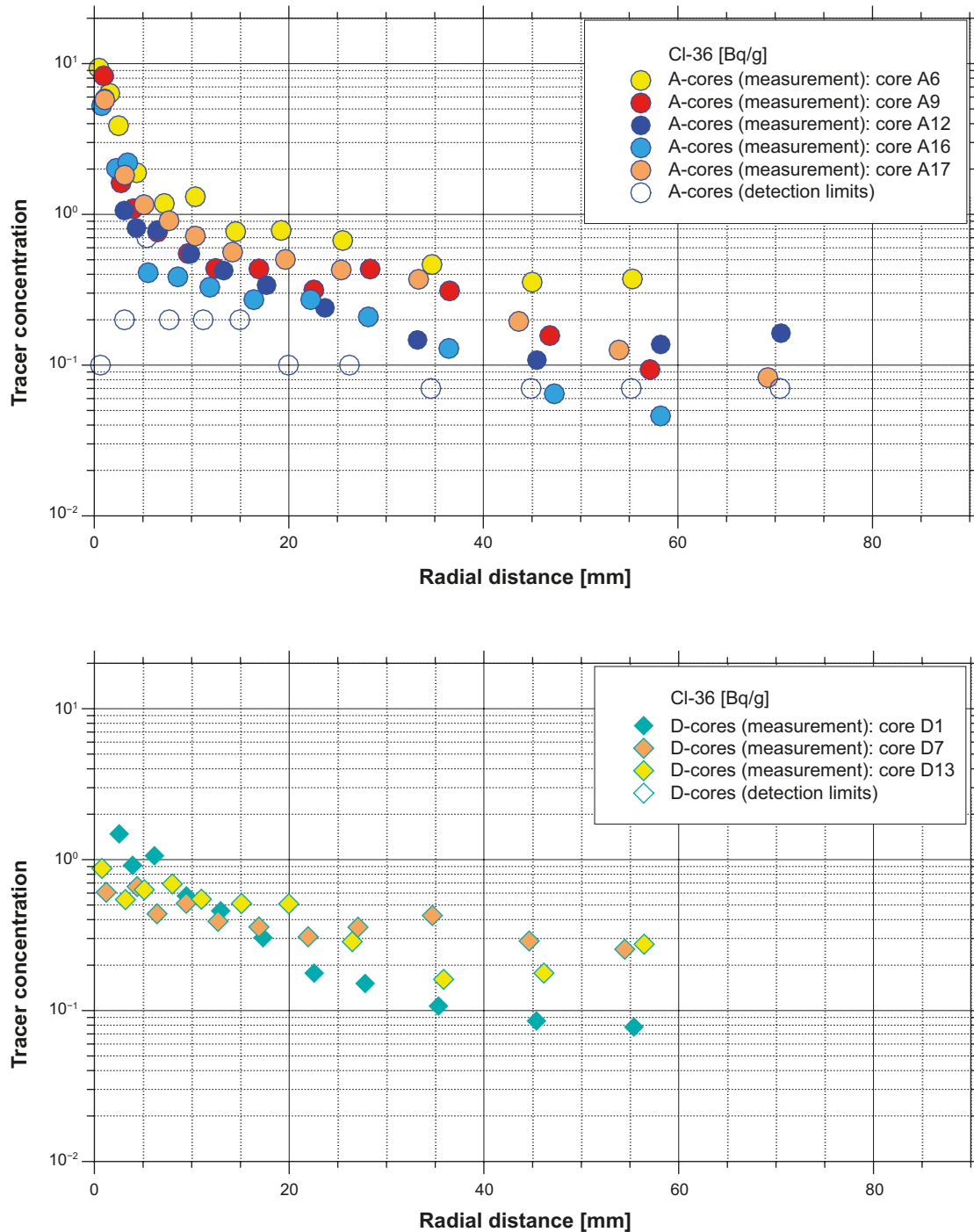

Figure A4-9. *Activity distributions in individual drill cores for ^{36}Cl$^-$; A-cores (top) and D-cores (bottom).*
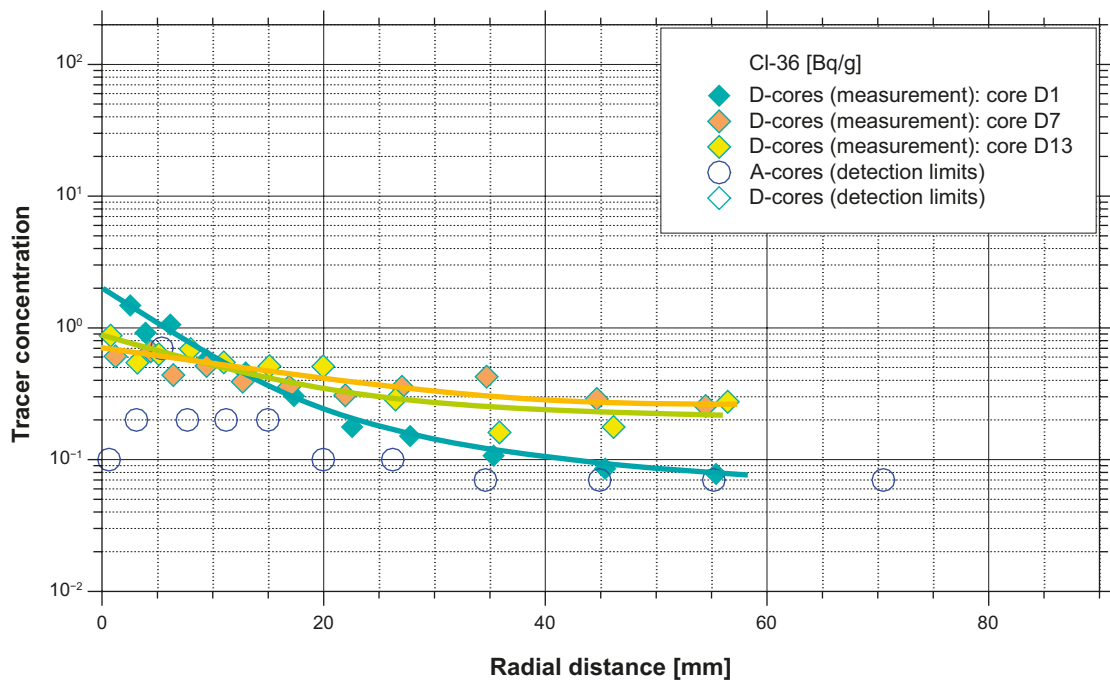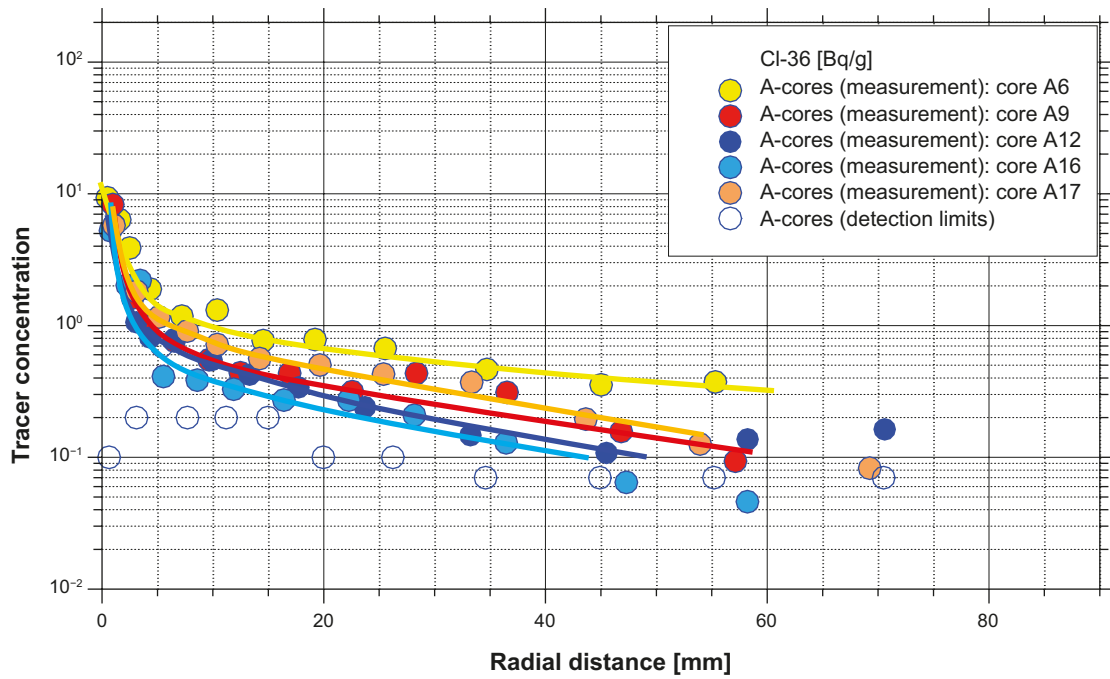
Figure A4-10. *Activity distributions and trends in individual drill cores for $^{36}Cl^-$; A-cores (top) and D-cores (bottom).*

SKB is responsible for managing spent nuclear fuel and radioactive waste produced by the Swedish nuclear power plants such that man and the environment are protected in the near and distant future.

skb.se